

ELECTRON-BOSON EFFECTS IN THE INFRARED PROPERTIES OF METALS

S. V. SHULGA

*Institute of Spectroscopy, RAS, Troitsk, 142190, Russia,
IFW-Dresden and the University of Bayreuth, Germany
(September 1998)*

The interpretation of optical conductivity in the normal and superconducting states is considered in the frame of the standard Isotropic Single wide Band (ISB) model using the theory proposed by Nam (Nam S.B., *Phys. Rev.* **156** 470-486 (1967)). The *exact analytical* inversion of the normal state Nam equations is performed and applied for the recovery of the reliable information from the experimental data. The Allen formula is derived in the strong coupling approximation and used for the physically transparent interpretation of the FIR absorption. The phenomenological "generalised" Drude formula is obtained from the Nam theory in a high temperature approximation. It is shown, that the reconstruction of the shape of the spectral function $\alpha^2 F(\omega)$ from the normal state optical data at $T > T_c$ is not unique and the same data can be fitted by many spectral functions. This problem is considered in detail from different points of view. At the same time, using the exact analytical solution, one can get from the normal state data a useful piece of information, namely, the value of the coupling constant, the upper energy bound of the electron-boson interaction function, and the averaged boson frequency. Moreover, they are even visually accessible, if the optical data are presented in term of the frequency dependent optical mass and scattering rate. The superconducting state Nam formalism and related simplified theory are analysed from the user point of view. A novel *adaptive* method of the *exact numerical inversion* of the superconducting state Nam equations is presented. Since this approach uses the *first derivative* from the experimental curve, the signal/noise ratio problem is discussed in detail. It is shown that, the fine structure of the spectral function can be recovered from optical data in the case of *s*-wave pairing symmetry. In contrast, in the *d*-wave case the resulting image is approximately the convolution of the input electron-boson interaction function and the Gauss distribution $\exp(-\omega^2/\Delta_{opt}^2)$. A simplified visual accessibility (VA) procedure is proposed for "by eye" analyses of the superconducting state optical reflectivity of the ISB metals with *s* and *d* pairing symmetry. The bosons, responsible for the superconductivity in $\text{YBa}_2\text{Cu}_3\text{O}_7$, exhibit a "phonon-like" spectral function with the upper frequency bound less than 500 cm^{-1} and the averaged boson frequency near 300 cm^{-1} .

I. INTRODUCTORY REMARKS, RESERVATIONS AND BASIC EQUATIONS

- This is the preliminary version of invited lecture for Nato-ASI "Material Science, Fundamental Properties and Future Electronic Applications of High-Tc Superconductors", Albena, Bulgaria, September 1998, Kluwer Academic Publishers, Dordrecht, pp. 323-360 (2001)
- The interpretation of the normal and superconducting state Far Infrared Region (FIR) properties of metals is still rather ambiguous. In this lecture I will restrict myself to the consideration of the of Isotropic Single wide Band (ISB) model based on the Nam formalism [1].
- From the optical conductivity $\sigma(\omega)$ one derives the so called transport spectral function $\alpha_{tr}^2 F(\omega)$. It has the same spectral structure, i.e. the same number of peaks with similar relative positions (see Fig.4 in [2] and Fig.1 in [3]) as a standard $\alpha^2 F(\omega)$ which enters the Eliashberg equations. But their amplitudes can be lower, and as a result the transport coupling constant λ_{tr} is less than the standard λ . In this lecture I will not distinct the $\alpha^2 F(\omega)$ and $\alpha_{tr}^2 F(\omega)$.
- If the electronic band is very narrow, the forward scattering could dominate. In this case the optical properties manifests themselves by the negligible coupling, while the tunnelling spectroscopy gives reasonable finite coupling strength. A similar problem arises when the quasiparticles from the flat or nested parts of the Fermi surface are mainly responsible for the superconductivity. Since they

have small Fermi velocities, their influence in the transport response function which is proportional to v_F^2 is weak. Such a scenario was recently proposed for borocarbides [4].

- In the frame of the Eliashberg theory it is impossible to elucidate the nature of the bosons which are responsible for the superconductivity. In this context I will use the term boson, keeping for short the standard electron-phonon notation $\alpha^2F(\omega)$.
- I will restrict myself to the consideration of the local (London) limit case, that is, to the normal skin effect scenario. The generalisation of results obtained to the nonlocal (Pippard) limit is possible but will not be considered here due to the lack of space.
- The power of the proposed methods is illustrated analysing available experimental data for a single-domain $\text{YBa}_2\text{Cu}_3\text{O}_{7-d}$ crystal [5]. Note, that to the best of my knowledge, the experimental HTSC superconducting state reflectivity was not been considered from the inverse problem viewpoint at all, despite the single early attempt [6].
- Theoretical analysis of any physical quantity, as optical conductivity, is performed in frame of some model which includes a theoretical formalism and some assumptions about the band structure, the anisotropy of the coupling function and so on. The considered here ISB model is the standard default. Nevertheless, in frame of its s -wave version the question: "What is the value of the gap?" has an unique answer, but for d -wave case the correct questions are either : "What are the values of the gaps?" " or "What is the value of the maximum gap? ". In other words, the absolute values and the physical meaning of the quantities are model dependent.
- If the model is reach enough, one can calculate many physical properties using the same *set of input (material) parameters*. A solution of the inverse problem means the determination of these material parameters from the experimental data. A short list of the ISB model input parameters is given in section I A.
- As a rule, the inverse problem is ill-posed. The experimental data contain less information, than we would like to know. The reasons for are the temperature induced broadening and the finite signal to noise ratio S/N.
- In this lecture we will mainly be interested in the amount of the remaining information about the spectral function $\alpha^2F(\omega)$, which can be obtained from the optical data. In spectroscopy the unit of information is a peak. A single peak needs four parameters for its description: the upper and the low frequency bounds Ω_{max} and Ω_{min} , the position of the maximum and its amplitude. An narrow symmetric peak within the broad band needs three parameters: the amplitude, the halfwidth, and the position. The sum of all peaks yields the upper and lower frequency bounds Ω_{max} and Ω_{min} of the spectral band. Since the Ω_{min} of the $\alpha^2F(\omega)$ is usually equal to zero, the remaining three band parameters of $\alpha^2F(\omega)$ can be determined even from the normal state data [7].

A. Isotropic single band model

The standard ISB model [8] is the most developed part of the modern theory of superconductivity. It describes *quantitatively* the renormalization of the physical properties of metals due to the electron-boson interaction. The input quantities of the ISB model are the density of states at the Fermi energy $N(0)$, the Fermi velocity v_F , the impurity scattering rate γ_{imp} , the Coulomb pseudopotential μ^* , and the spectral function $\alpha^2F(\omega)$ of the electron-boson interaction. The scale of transport and optical properties is fixed by the plasma frequency $\hbar\omega_{pl} = \sqrt{4\pi e^2 v_F^2 N(0)}/3$. In this section I present only the final expressions of the Nam theory, more detailed information can be found in [1,2,9].

In order to calculate any physical property in the superconducting state one needs a solutions of Eliashberg equations (EE) [11]. In my opinion, the following EE representation is most suitable for numerical solution by iterations

$$\begin{aligned}
Im\tilde{\Delta}(\omega) &= \frac{i\gamma_{imp}}{2} \frac{\tilde{\Delta}(\omega)}{\sqrt{\tilde{\omega}^2(\omega) - \tilde{\Delta}^2(\omega)}} + \frac{\pi}{2} \int dy \alpha^2 F(\omega - y) \\
&\quad \left[\coth\left(\frac{\omega - y}{2T}\right) - \tanh\left(\frac{y}{2T}\right) \right] \operatorname{Re} \frac{\tilde{\Delta}(y)}{\sqrt{\tilde{\omega}^2(y) - \tilde{\Delta}^2(y)}}
\end{aligned} \tag{1}$$

$$\begin{aligned}
Im\tilde{\omega}(\omega) &= \frac{i\gamma_{imp}}{2} \frac{\tilde{\omega}(\omega)}{\sqrt{\tilde{\omega}^2(\omega) - \tilde{\Delta}^2(\omega)}} + \frac{\pi}{2} \int dy \alpha^2 F(\omega - y), \\
&\quad \left[\coth\left(\frac{\omega - y}{2T}\right) - \tanh\left(\frac{y}{2T}\right) \right] \operatorname{Re} \frac{\tilde{\omega}(y)}{\sqrt{\tilde{\omega}^2(y) - \tilde{\Delta}^2(y)}},
\end{aligned} \tag{2}$$

where $\tilde{\Delta}(\omega)$ and $\tilde{\omega}(\omega)$ are the renormalized gap function and the renormalized frequency respectively, and γ_{imp} denotes the impurity scattering rate within the Born approximation. The real and the imaginary parts of the Eliashberg functions $\tilde{\Delta}(\omega)$ and $\tilde{\omega}(\omega)$ are connected by the Kramers-Kronig relations. Hence, they have the same Fourier images. This reasoning yields the fast solution procedure. The convolution type integrals (1-2) should be calculated by the Fast Fourier Transform (FFT) algorithm. The inverse *complex* Fourier transformations of the results obtained give *complex* values of $\tilde{\Delta}(\omega)$ and $\tilde{\omega}(\omega)$. If one would like to use this efficient FFT method also for *d*-wave pairing symmetry, the process of arithmetic-geometric mean [12] for the evaluation of the complex elliptic integrals (see below Eqs. (67,68) is strongly recommended. The density of states $\operatorname{Re}N(\omega)$ and the density of pairs $\operatorname{Re}D(\omega)$

$$N(\omega) = \frac{\tilde{\omega}(\omega)}{\sqrt{\tilde{\omega}^2(\omega) - \tilde{\Delta}^2(\omega)}}, \tag{3}$$

$$D(\omega) = \frac{\tilde{\Delta}(\omega)}{\sqrt{\tilde{\omega}^2(\omega) - \tilde{\Delta}^2(\omega)}}, \tag{4}$$

could be approximated by step functions. The convolution of any spectrum with the step function $\operatorname{sign}(y^2 - \Delta_0^2)$ results in the shift by Δ_0 at $y > 0$ and by $-\Delta_0$ at $y < 0$ and its integration over y . It is important, that due to the presence of singularities in $N(\omega)$ and $D(\omega)$ at $\omega = \Delta_0$ the more complicated functions such as $\int d\omega' N(\omega')N(\omega - \omega')$ and $\int d\omega' D(\omega')D(\omega - \omega')$ still contain a jump (now at $\omega = 2\Delta_0$). Since the convolution is a quite general property of the Green functions approach, one can expect that the first derivatives from a spectrum (of different nature) over frequency will reproduce the input spectral function $\alpha^2 F(\omega)$ (may be with the appropriate phase distortion). When applied to the optical conductivity, this approach gives visual accessibility (VA) procedure discussed in the sec. III.

In the normal state the set (2) is reduced to the following simple formula

$$Im\tilde{\omega}(\omega) = \frac{\gamma_{imp}}{2} + \frac{\pi}{2} \int dy \alpha^2 F(y) \left[\coth\left(\frac{y}{2T}\right) - \tanh\left(\frac{\omega - y}{2T}\right) \right], \tag{5}$$

which however looks unwieldy in comparison with the same formula presented in Matsubara formalism

$$\tilde{\omega}(i\omega_n) \equiv \tilde{\omega}_n = \tilde{\omega}_{n-1} + 2\pi T(1 + \lambda_n) \tag{6}$$

where

$$\lambda_k \equiv \alpha^2 F(i\nu_k) = 2 \int dz \alpha^2 F(z) z / (z^2 + \nu_k^2) \tag{7}$$

are kernels of the spectral function, $\omega_k = \pi T(2k + 1)$ and $\nu_k = 2\pi T k$ are fermion (ω_k) and boson (ν_k) Matsubara energies, respectively, and $\tilde{\omega}_0 = \gamma_{imp}/2 + \pi T(1 + \lambda_0)$.

The normal state ISB optical conductivity takes the following forms

$$\sigma(\omega, T) = \frac{\omega_{pl}^2}{8\pi i\omega} \int dy \frac{\tanh\left(\frac{y+\omega}{2T}\right) - \tanh\left(\frac{y}{2T}\right)}{\tilde{\omega}(\omega + y) - \tilde{\omega}^*(y)}, \tag{8}$$

and

$$\sigma(i\omega_n, T) \equiv \sigma_n = \frac{\omega_{pl}^2}{4\pi n} \sum_{k=0}^{n-1} \frac{1}{\tilde{\omega}_k + \tilde{\omega}_{n-k-1}}, \quad (9)$$

in the real and imaginary axes techniques, respectively.

The tedious expression for the superconducting state ISB optical conductivity has the form [1,9,10]

$$\begin{aligned} \sigma(\omega) = & \frac{\omega_{pl}^2}{16\pi\omega} \int dx \frac{g_{rr} \tanh(x/2T)}{\sqrt{\tilde{\Delta}^2(x) - \tilde{\omega}^2(x)} + \sqrt{\tilde{\Delta}^2(x+\omega) - \tilde{\omega}^2(x+\omega)}} \\ & - \frac{g_{rr}^* \tanh[(x+\omega)/2T]}{\left(\sqrt{\tilde{\Delta}^2(x) - \tilde{\omega}^2(x)} + \sqrt{\tilde{\Delta}^2(x+\omega) - \tilde{\omega}^2(x+\omega)}\right)^*} \\ & + \frac{g_{ar} \{\tanh[(x+\omega)/2T] - \tanh(x/2T)\}}{\sqrt{\tilde{\Delta}^2(x) - \tilde{\omega}^2(x)} + \left(\sqrt{\tilde{\Delta}^2(x+\omega) - \tilde{\omega}^2(x+\omega)}\right)^*}, \end{aligned} \quad (10)$$

where

$$\begin{aligned} g_{rr} &= 1 - N(x)N(x+\omega) - D(x)D(x+\omega), \\ g_{ra} &= 1 + N^*(x)N(x+\omega) + D^*(x)D(x+\omega) \end{aligned} \quad (11)$$

are *coherent factors*.

II. NORMAL STATE OPTICAL CONDUCTIVITY

A. The exact solution of an inverse problem

It is amusing, that the Eq. (9) is solvable for $\tilde{\omega}_k$ and Eq. (6) for λ_k . Hence, at least theoretically, an exact analytical solution exists. It takes three or four steps as shown below.

I) One has to perform the analytical continuation of the conductivity $\sigma(\omega)$ from the real energy axis, where we are living, to the poles of the Bose distribution function (Matsubara boson energies) $i\nu_k = 2\pi iTk$. This procedure is similar to the Kramers-Kronig analysis, which is nothing other than the analytical continuation from the real frequency axis to itself. For example, if one fits the data by a sum of Drude and Lorentz terms or by formula (33), one has simply to substitute the complex values $i\nu_k$ for the frequency. Note, that the non-metallic (IR active direct phonon contribution and interband transition) part of the dielectric permeability $\epsilon_{ph}(\omega)$ have to be subtracted from the total one $\epsilon(\omega)$ before starting of the analysis. In the genuine far infrared region one could use the real constant $\epsilon_\infty = \epsilon_{ph}(0)$, instead of $\epsilon_{ph}(\omega)$, but if the spectral range is wide, the subtraction of $\epsilon_{ph}(\omega)$ is not trivial.

II) The renormalized frequencies should be calculated from (9) as follows

$$\tilde{\omega}_0 = \frac{\omega_{pl}^2}{8\pi\sigma_1}, \quad (12)$$

$$\tilde{\omega}_1 = \frac{\omega_{pl}^2}{4\pi\sigma_2} - \tilde{\omega}_0, \quad (13)$$

$$\tilde{\omega}_{n-1} = \frac{\omega_{pl}^2}{2\pi A_n} - \tilde{\omega}_0, \text{ where } A_n = \sigma_n - \frac{\omega_{pl}^2}{4\pi n} \sum_{k=1}^{n-2} \frac{1}{\tilde{\omega}_k + \tilde{\omega}_{n-k-1}}. \quad (14)$$

III) Inverting Eq. (6), one could evaluate the values of the spectral function $\lambda_n = \alpha^2 F(\nu_n)$ we looked for

$$\lambda_0 = \frac{\tilde{\omega}_0 - \gamma_{imp}/2}{\pi T} - 1 \quad (15)$$

$$\lambda_n = \frac{\tilde{\omega}_n - \tilde{\omega}_{n-1}}{2\pi T} - 1. \quad (16)$$

IV) Using, for example, Pade polynomials [14] one has to continue the electron-boson interaction function back to the real axis.

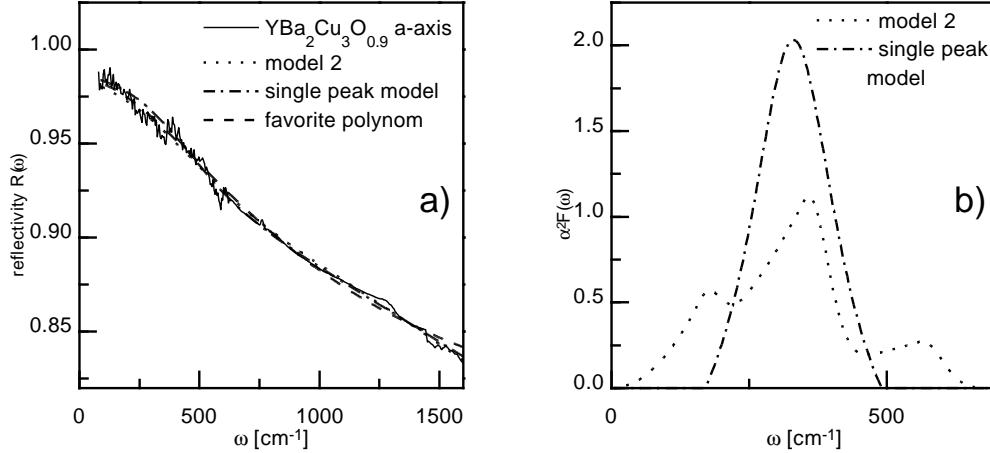


FIG. 1. Panel (a) shows the frequency dependence of the normal state reflectivity (solid line, $T=100$ K, Schützmann J. et al., *Phys. Rev.*, **B46**, 512 (1992)) in comparison with the model ones. The curves, shown by the dotted and the dotted-dashed lines, was calculated using "model 2" and "single peak" spectra (presented on the panel (b)). The dashed line is the least square fit of $\text{YBa}_2\text{Cu}_3\text{O}_{0.9}$ a-axis reflectivity by the favourite polynomial Eq. 32 (with the fixed $\epsilon_\infty = 12$).

In practice, if the signal to noise ratio is not extremely large, the last step makes no sense due to the dramatic increase of the uncertainty in the λ_n with elevation of n . The point is that the small quantities λ_n Eq. (16) and A_n Eq. (14) are the difference of large quantities. Note, that the uncertainty in the λ_n values has to be small, not in comparison with λ_n itself, but with the difference between λ_n and its high energy asymptotic value

$$\tilde{\lambda}_n = \frac{2\lambda_0 \langle \Omega^2 \rangle}{\langle \Omega^2 \rangle + \nu_n^2} \quad (17)$$

where

$$\langle \Omega^2 \rangle = \frac{1}{\lambda_0} \int_0^\infty d\Omega \Omega \alpha^2 F(\Omega) \quad (18)$$

If the average boson energy has the order of $2\pi T$, the last condition ($\delta\lambda_n \ll |\tilde{\lambda}_n - \lambda_n|$) may be violated even for $n=3$, since $\tilde{\lambda}_n$ and λ_n have similar values. For example, at $T=100$ K for the spectral function, shown by the dotted line in Fig. 1, $\tilde{\lambda}_n/\lambda_n=1.37, 1.12, 1.06, 1.03$ for $n=1, 2, 3, 4$ respectively. Three or four λ_n values only form a too small parameter set to recover correctly the shape of the spectral function. Actually, the possibility to obtain at least small amount of reliable information, is the additional advantage provided by the Matsubara solution in comparison with the real axis one where *all* values are unreliable [15]. Fig. 1 shows the good agreement between the experimental normal state 1-2-3 single crystal reflectivity data [5] and the calculated ones using for *various* spectral functions. Unfortunately, the lack of a unique solution promoted unreasonable speculations on the mechanisms in several novel superconducting systems in connection with proposed hand-made electron-boson interaction functions. In my opinion, twelve years after the discovery of the superconductivity in cuprates it is timely to return to a self-consistent description of the superconductivity in this compounds.

The first Matsubara value of the conductivity $\sigma(i\nu_1)(\equiv \sigma_1)$ gives the value of the coupling constant $\lambda(\equiv \lambda_0)$, if the plasma frequency ω_{pl} and the impurity scattering rate γ_{imp} are known *a priori*

$$\frac{1}{\sigma_1} = \frac{8\pi^2 T(1 + \lambda_0)}{\omega_{pl}^2} + \frac{4\pi\gamma_{imp}}{\omega_{pl}^2}. \quad (19)$$

The reflectivity $R(\omega)$ can also be continued to the imaginary frequency axis and included into the solution of the inverse problem. Following this way, one can derive from (19) the following formula

$$\lambda_0 = -\frac{\gamma_{imp}}{2\pi T} - 1 + \frac{\omega_p^2}{(2\pi T)^2(\coth^2(K_1/4) - \epsilon_\infty)}, \quad (20)$$

where ϵ_∞ is the low-frequency value of the non-metallic (phonon and interband transition) part of dielectric permeability, and K_m is the electromagnetic kernel

$$K(\nu_m) = \frac{2\nu_m}{\pi} \int_0^\infty dz \frac{\log|1 - R(z)|}{z^2 + \nu_m^2}. \quad (21)$$

The first λ_1 and the second λ_2 allow (for example) to estimate the average boson energy and *very approximately* the width of the spectral function. If there is the possibility to combine this incomplete information about $\alpha^2 F(\omega)$ with the results of other spectral measurements, for example, tunnelling or neutron data, one can qualify the transport spectral function. The so called "model 2" electron-boson interaction function [7] was recovered assuming, that the solution has to be resemble the phonon density of states, measured by inelastic neutron spectroscopy.

B. Optical mass and impurity scattering rate

In ref. [7,15] we shown, that it is useful to describe the optical conductivity in terms of the so called "extended" Drude formula

$$\sigma(\omega, T) = \frac{\omega_{pl}^2/4\pi}{W(\omega, T)} = \frac{\omega_p^2/4\pi}{\gamma_{opt}(\omega, T) - i\omega m_{opt}^*(\omega, T)/m_b}. \quad (22)$$

Here the optical relaxation $W(\omega)$, the optical mass $m_{opt}^*(\omega, T)/m_b$ and the optical scattering rate $\gamma_{opt}(\omega, T)$ as the complex, real and imaginary parts of an inverse normalised conductivity $\omega_{pl}^2/4\pi\sigma(\omega, T)$ have been introduced. This presentation is old and popular in spectroscopy, but the practical value of the Eq. (22) has not been exploited much. The optical relaxation will be compared with the effective mass $m_{eff}^*(\omega, T)/m_b$ and the effective scattering rate $\gamma_{eff}(\omega, T)$, which by definition are the real and imaginary parts of the renormalized frequency

$$\tilde{\omega}(\omega, T) = \frac{\omega m_{eff}^*(\omega, T)}{m_b} + \frac{i\gamma_{eff}(\omega, T)}{2}. \quad (23)$$

When the frequency dependencies of $\gamma_{opt}(\omega, T)$ and $m^*(\omega, T)/m_b$ are plotted, the coupling constant, the average boson energy and the upper boundary of spectral function are visually accessible (see Fig. 2). The appropriate visual accessibility rules can be derived from the properties of the renormalized frequency $\tilde{\omega}$ using the Allen formula Eq. (26) [2]. Since such useful expression was originally obtained in the weak coupling approximation ($\lambda \ll 1$) only, below I rederive it for the general case, including strong coupling.

For any k the values of λ_k are positive and are of the same order of magnitude, except may be λ_0 . It means, that in the zero order the series $\tilde{\omega}_n$ defined by Eq. (6) is an arithmetical progression. Consequently, according to the Gauss rule for the arithmetical series the denominators $\tilde{\omega}_k + \tilde{\omega}_{n-k-1}$ in (9) at a given n do not depend on k , that is, they coincide. In view of Eq. (22), Eq. (9) takes the form

$$W_{n+1} \approx \tilde{\omega}_k + \tilde{\omega}_{n-k}. \quad (24)$$

Hence we can expand the denominator in (9)

$$\frac{4\pi\sigma_n}{\omega_{pl}^2} \equiv \frac{1}{W_n} = \frac{1}{n} \sum_{k=0}^{n-1} \frac{1}{W_n [1 + (\tilde{\omega}_k + \tilde{\omega}_{n-k-1} - W_n)/W_n]} \quad (25)$$

to the first order in power of $(\tilde{\omega}_k + \tilde{\omega}_{n-k-1} - W_n)/W_n$. After some simple algebra we arrive at the sought-for Allen formula

$$W_n = \frac{2}{n} \sum_{k=0}^{n-1} \tilde{\omega}_k. \quad (26)$$

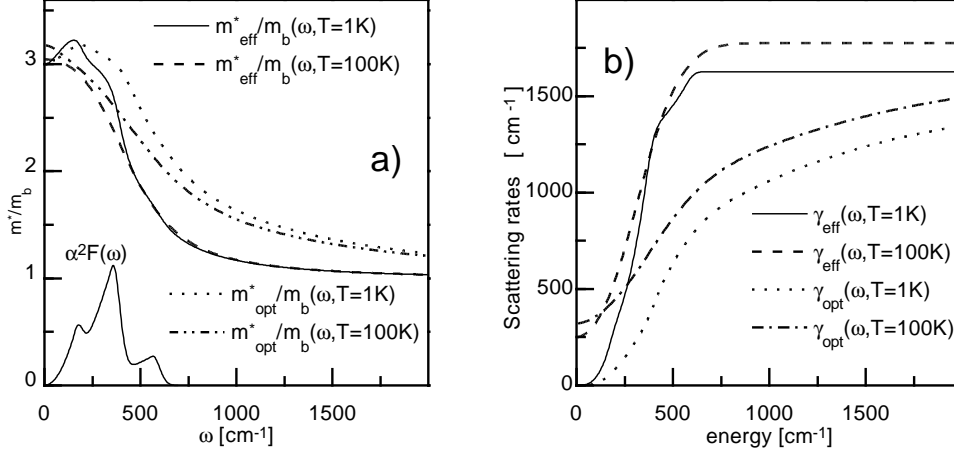


FIG. 2. The frequency dependencies of the normal state optical and effective masses (a) and scattering rates (b) calculated using the "model 2" spectral function with $\lambda=2$ (shown in panel (a) for comparison). The quasiparticle effective mass $m_{eff}^*(\omega)/m_b$ and scattering rate $\gamma_{eff}(\omega)$ at $T=1$ K (solid lines, panels (a) and (b)) reproduce the fine structure of the spectral function, but at $T=100$ K (dashed lines) this function are smeared out due to averaging over Fermi distribution. At $\omega > \Omega_{max}$ the quasiparticles become "undressed", $m_{eff}^*(\omega)/m_b \approx 1$ and $\gamma_{eff}(\omega) \approx const$. The optical mass $m_{opt}^*(\omega)/m_b$ and the scattering rate $\gamma_{opt}(\omega)$ even at $T=1$ K (dotted lines) do not reproduce the structure of the spectral function due to the energy averaging, all the more at high temperature ones ($T=100$ K, dashed-dotted lines).

The real axis versions of Eq. (26) at $T=0$ look similar

$$W(\omega) = \frac{1}{\omega} \int_0^\omega dz 2\tilde{\omega}(z), \quad (27)$$

$$\frac{\omega m_{opt}^*(\omega, T)}{m_b} = \frac{1}{\omega} \int_0^\omega dz \frac{2zm_{eff}^*(z, T)}{m_b}, \quad (28)$$

$$\gamma_{opt}(\omega) = \frac{1}{\omega} \int_0^\omega dz \gamma_{eff}(z). \quad (29)$$

and justify the following simple description of the interaction of light with the conducting subsystem of the normal state metal. When a photon with an energy ω has been absorbed, *two* excited *virtual* quasiparticles, an "electron" and a "hole" are created. If the first particle's frequency is ω' , the second ones frequency should be $\omega - \omega'$. The excited "electron" and "hole" relax to the Fermi level according to the quasiparticle laws (see Eqs. 5,6). Since ω' can varies from 0 to ω , the optical relaxation $W(\omega)$ is the frequency-averaged ($\frac{1}{\omega} \int_0^\omega$), double (electron+hole \rightarrow factor 2) renormalized frequency $\tilde{\omega}$.

At $T=0$ the ISB effective scattering rate $\gamma_{eff}(\omega) \equiv 2Im\tilde{\omega}(\omega)$

$$\gamma_{eff}(\omega) = \gamma_{imp} + 2\pi \int_0^\omega dy \alpha^2 F(y) \quad (30)$$

has a clear physical meaning. The excited quasiparticles with the energy ω can relax by the emission of virtual bosons with the energy varying the range from 0 to ω or by the impurity scattering.

At finite temperature the Allen formula

$$W(\omega) = \frac{1}{\omega} \int dz \frac{\tanh\left(\frac{\omega-z}{2T}\right) + \tanh\left(\frac{z}{2T}\right)}{2} 2\tilde{\omega}(z) \quad (31)$$

and the effective scattering rate (5) have exactly the same interpretation, since the only difference between them and Eqs. (27,27,29,30) is the presence of the Fermi distributions instead of step functions at $T=0$.

Figure 2 shows the frequency dependencies of the normal state optical and effective masses and scattering rates calculated using the model spectral function [7] with $\lambda=2$. The results are plotted for the low temperature $T=1$ K and for $T=100$ K which is close to T_c and has the order of $\Omega_{boson}/2\pi T$, where $\Omega_{boson}=330$ cm⁻¹ is the averaged boson frequency. Both $m_{eff}^*(\omega)/m_b$ and $\gamma_{eff}(\omega)$ show the characteristic features corresponding the peculiarities of the phonon spectrum. When the frequency ω exceeds the upper energy bound of the boson spectrum Ω_{max} , the quasiparticle becomes "undressed". Its mass $m_{eff}^*(\omega)/m_b \approx 1$ and effective scattering rate $\gamma_{eff}(\omega) \approx const$, but of course, the absolute value of $\gamma_{eff}(\omega \rightarrow \infty)$ could be huge.

The optical mass $m_{opt}^*(\omega)/m_b$ and scattering rate $\gamma_{opt}(\omega)$ have no features at $\omega \approx \Omega_{max}$ due to the energy averaging (27,28,29,31). One can only *calculate* the approximate value of Ω_{max} as the frequency where the $m_{opt}^*(\omega)/m_b - 1$ and $\gamma_{opt}(\omega)$ reach the halves of their maximum magnitudes. Fig. 2 shows, that this my rule can not be applied even to the calculated frequency dependence of the optical scattering rate $\gamma_{opt}(\omega)$, the more to the experimental curve, where *the high energy* behaviour is distorted by the interband transition contribution to the dielectric permeability. In contrast the frequency dependence of the optical mass $m_{opt}^*(\omega)/m_b$ is suitable for the application of the simple criterion

$$m^*(\omega = \Omega_{max})/m_b - 1 \approx 0.5(m^*(\omega = 0)/m_b - 1). \quad (32)$$

Moreover its *low energy* value $m_{opt}^*(\omega = 0)/m_b \approx 1 + \lambda_{tr}$ itself contains a useful piece of information. Fig. 2a shows, that the approximate values of the transport coupling constant $\lambda_{tr} \approx (m_{opt}^*(0)/m_b - 1)$ and the upper frequency bound of the electron-boson coupling function [$m_{opt}^*(\Omega_{max})/m_b - 1 \approx 0.5(m_{opt}^*(0)/m_b - 1)$] are visually accessible. If the spectral function is wide and its peak position (or averaged frequency) coincide roughly with the $\Omega_{max}/2$, the optical relaxation $W(\omega)$ is smooth and the elucidation of Ω_{boson} at high temperature is impossible. When an exotic superconductor with the narrow, δ -function like spectral function will be discovered, following this way one can easily construct the recipe for the evaluation of the strength and the position of the single peak.

C. My favourite polynomial

The Pade polynomial analytical continuation [14] is a capricious and not completely correct procedure. Nevertheless, if the temperature is high enough in comparison with the energy under consideration it works splendidly. The numerical experiment has given to my great surprise the following (and to some extent obvious) result (see Fig. 3). The good agreement between the real axis calculations and the Matsubara ones takes place every time when the approximation using 1000 σ_n points gives the same result as the *four* points Pade approximation.

This remarkable Pade polynomial with only four parameters $\omega_{pl}^2/4\pi$, A , B and C

$$\sigma(\omega) = \frac{\omega_{pl}^2/4\pi}{A - i\omega + \frac{B\omega}{\omega + iC}} \quad (33)$$

fits well the majority of the experimental data at $T \geq T_c$ and itself is the demonstration of the result obtained in section II A: the few first Matsubara values σ_k are responsible for the frequency dependence of $\sigma(\omega)$.

The Pade polynomial (33) is a formula of merit. At first, it has the correct analytical properties. Its two poles are located in the lower half-plane of the complex energy. The high ($\omega \rightarrow \infty$) and low ($\omega \rightarrow 0$) energy asymptotic behaviour are reasonable [23]. At second, it is ideal for the least square

fits of experimental $R(\omega)$ [24], as well as for simple analytical estimations. Having the exact solution (see sec.IIA) we have to substitute the complex values $i\nu_k$ for energy, perform easily the analytical continuation to the imaginary axis and analyse the values of σ_i . In the way we obtain the interpretation of A, B, C. Another possibility is a fast and easy analysis of the data in terms of the optical mass $m_{opt}^*(\omega, T)/m_b$ and the optical scattering rate $\gamma_{opt}(\omega, T)$

$$\frac{m_{opt}^*(\omega, T)}{m_b} - 1 = \frac{BC}{\omega^2 + C^2} \quad (34)$$

$$\gamma_{opt}(\omega, T) = A + \frac{B\omega^2}{\omega^2 + C^2}. \quad (35)$$

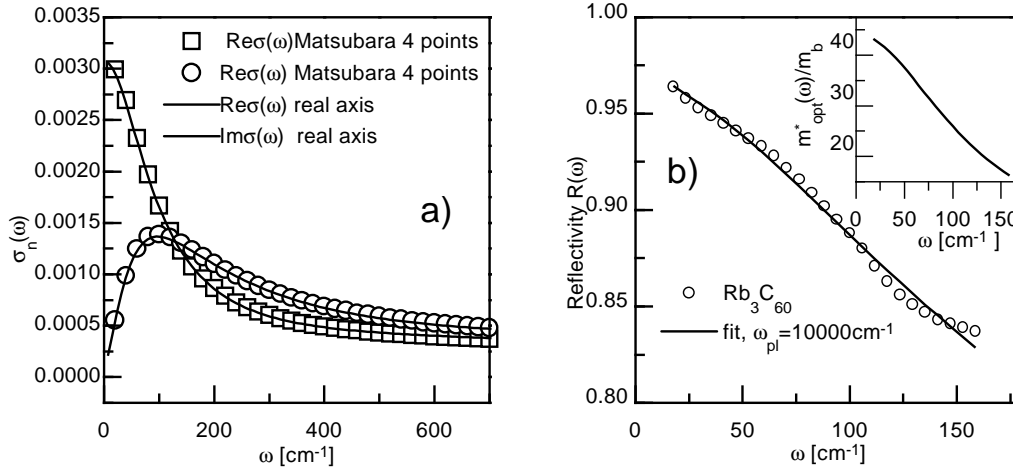


FIG. 3. Panel (a) shows the frequency dependencies of the real and imaginary parts of the calculated normal state optical conductivity using the real axis formalism (solid lines) and Matsubara technique (squares - $\text{Re}\sigma(\omega)$, circles - $\text{Im}\sigma(\omega)$). The analytical continuation from the imaginary axis to the real one was made by the Pade polynomial with the degree of polynomial $n=4$. Calculations was made for $T=100$ K using "model 2" spectral function. Panel (b) shows the frequency dependence of the normal state reflectivity $R(\omega)$ of Rb_3C_{60} measured at $T=40$ K by Degiorgi *et al.*, *Phys. Rev. Lett.* **69**, 2987 (1992) (circles) in comparison with the least square fit by the favourite polynomial. Since four parameters were too much, the value of the plasma frequency $\omega_{pl}=10000$ cm^{-1} was fixed. The obtained frequency dependence of the optical mass is shown in the inset.

At third, if the low-frequency reflectivity $R(\omega)$ measured at high temperature can not be fitted by Eq. (33) or the obtained value of λ_0 contradicts the generally accepted values, it might indicate, that the material under consideration is *not* a standard Isotropic Single wide Band (ISB) metal and its properties have to be analysed in terms of *another*, unconventional model. In order to illustrate the utility of this approach, let us consider another superconducting compound with relatively high transition temperature Rb_3C_{60} [16,18,17]. Since the ratio of the experimental reflectivities in the superconducting and normal states $R_s/R_n \approx 1$ above 100 cm^{-1} [16], in frame of the ISB model it means, that the high energy bound of the electron-boson interaction function $\Omega_{max} < 100$ cm^{-1} . The low energy part of the normal state reflectivity $R(\omega)$, measured at $T=40$ K, was fitted (with the adopted fixed $\omega_{pl}=10000$ cm^{-1}) by (33) (see Fig. 3b), $m_{opt}^*(\omega, T)/m_b$ is shown in the inset. One can see, that the optical mass at small ω is huge itself and gives $\lambda > 100$. This value points to heavy fermion or polaron models, rather than to the generally accepted weak or intermediate coupling scenario. On the other hand, the analysis of the normal state specific heat data gives an extremely small value of the coupling constant. As a result we concluded that Rb_3C_{60} is not a ISB metal and its properties should be treated in terms of a more complicated model which takes into account the self-energy and conductivity vertex corrections, the small value of the bandwidth $\Delta E \approx 100$ meV, possible influence of the electron-electron correlation, the strong anisotropy of the coupling function and the Fermi velocity, and etc.

And the last but not least, if the data can be fitted by (33), that is by the formula with four parameters,

it is impossible to recover from this *four* parameters the detailed shape of the electron-boson interaction function $\alpha^2 F(\omega)$.

In conclusion, it is naturally to define the amount of the available information by the number of poles and zeros of the function which fits well the experimental curve or the number of the determinate Matsubara values.

D. Temperature dependence of the optical mass and relaxation rate and its two-band ersatz

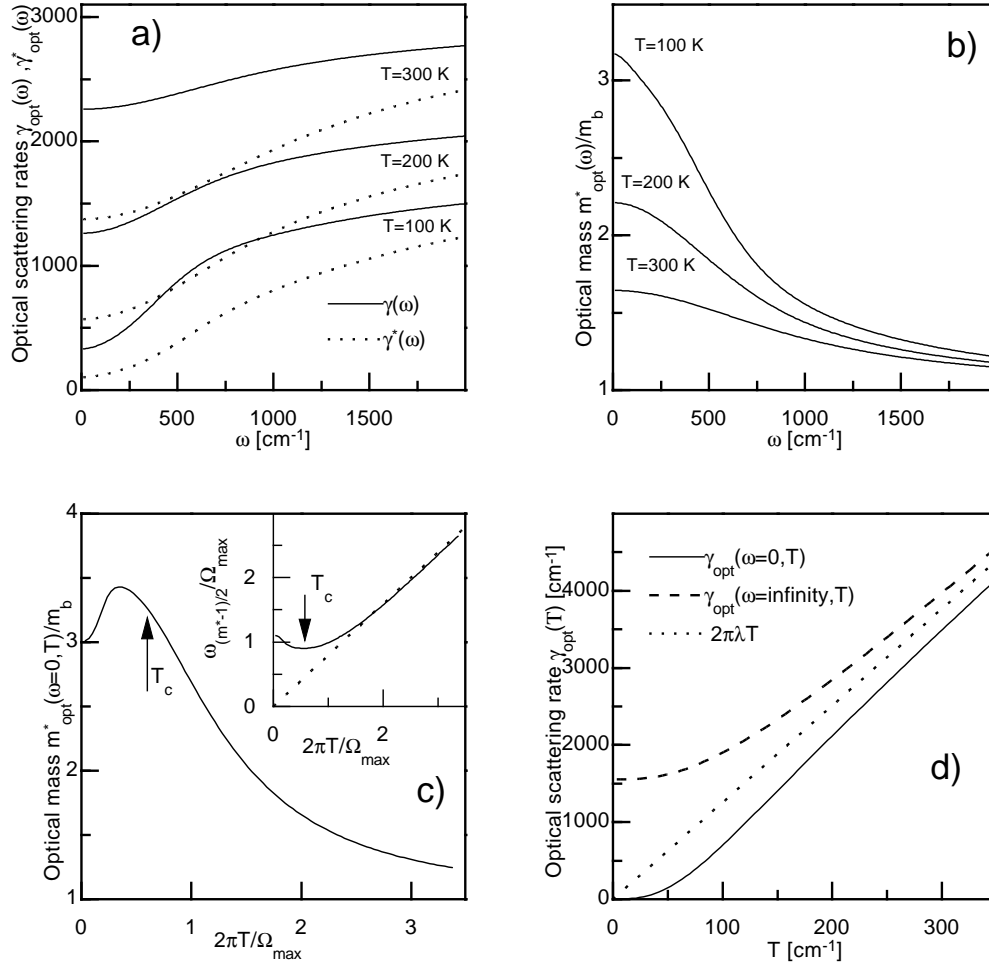


FIG. 4. Panels (a) and (b) show the frequency dependence of the optical mass and the optical scattering rate for $T=100\text{K}$, 200K , 300K . Panels (c) and (d) present the corresponding temperature dependence of $m_{opt}^*(T)/m_b$ and $\gamma_{opt}(T)$ for $\omega = 0$ and $\omega = \infty$. All curves (solid lines) was calculated using model 2 spectral function. For comparison the normalised optical scattering rates $\gamma^*(\omega, T) = \gamma_{opt}(\omega, T)/m_{opt}^*(\omega, T)/m_b$ are plotted by dotted lines in panel (a). The temperature dependence of the quantity $\omega_{(m^*-1)/2}$ (see text) is shown by solid line on inset (c) together with the phenomenological line $\omega = 5T$ (dotted line). The common for $\gamma_{opt}(\omega = 0, T)$ and $\gamma_{opt}(\omega = \infty, T)$ asymptote $\gamma = 2\pi\lambda T$ is shown by dotted line in panel (d).

In frame of the ISB model we assume, that all quasiparticles have the same Fermi velocity, but in real metals there is some anisotropy of v_F . If the impurity scattering rate γ_{imp} is small in comparison with the complete optical scattering rate γ_{opt} and the electron-boson coupling is isotropic, we can use the average value $\langle v_F^2 \rangle$ and keep the ISB model. On the other hand, if the impurity scattering, given

by the mean free path l , dominates, the quasiparticles from different parts of the Fermi surface will have different scattering rates $\gamma_{imp,i} = v_{F,i}/l$. Let us accept for simplicity, that we can divide the Fermi surface between two parts with the approximately uniform properties. The optical conductivity of this two-band system is the sum of two Drude terms

$$\sigma(\omega) = \frac{\omega_{pl,1}^2/4\pi}{\gamma_1 - i\omega} + \frac{\omega_{pl,2}^2/4\pi}{\gamma_2 - i\omega}. \quad (36)$$

One can see, that Eq. (36) and Eq. (33) are equivalent and four parameters $\omega_{pl,1}^2, \omega_{pl,2}^2, \gamma_1, \gamma_2$ in (36) connected with ω_{pl}^2, A, B, C in (33) as follows

$$\begin{aligned} \omega_{pl}^2 &= \omega_{pl,1}^2 + \omega_{pl,2}^2 \\ C &= \frac{\omega_{pl,1}^2 \gamma_2 + \omega_{pl,2}^2 \gamma_1}{\omega_{pl,1}^2 + \omega_{pl,2}^2} \\ A &= \frac{\gamma_1 \gamma_2 (\omega_{pl,1}^2 + \omega_{pl,2}^2)}{\omega_{pl,1}^2 \gamma_2 + \omega_{pl,2}^2 \gamma_1} \\ B &= \gamma_1 + \gamma_2 - A - C \end{aligned} \quad (37)$$

It means, that even if there is no electron-boson interaction in the two-band system, the frequency dependence of its optical conductivity (36) will reproduce a ISB model one (8) with some frequency dependent "mass" and "scattering rate". The multiband ersatz of the electron-boson effects could be revealed by the investigation of the temperature dependence of $m_{opt}^*(\omega, T)/m_b$ and $\gamma_{opt}(\omega, T)$. It originates mainly from the presence of the Bose factor in Eqs.(5) (\equiv sampling in (6)) and to a less degree from the Fermi distributions in Eqs. (5-9).

In subsection IIB the low ($T \rightarrow 0$) temperature behaviour of $m_{opt}^*(\omega)/m_b$ and $\gamma_{opt}(\omega)$ was discussed in detail. We found, that at a given quasiparticle frequency ω in accord with the frequency conservation principle only virtual bosons with $\Omega < \omega$ can contribute to the relaxation.

At high temperature the bosons lose their individuality. At $T \rightarrow \infty$ the expression (5) can be substantially simplified, since the Bose factor $coth(z/2T) \approx 2T/z$ dominates in comparison with the Fermi one $tanh[(\omega - z)/2T]$. Keeping the leading term $2T/z$ we arrive at

$$Im\tilde{\omega}(\omega) \equiv \gamma_{eff}(\omega) \approx \frac{\gamma_{imp}}{2} + \pi T \int \frac{dy \alpha^2 F(y)}{y} = \frac{\gamma_{imp} + 2\pi\lambda T}{2}. \quad (38)$$

In Matsubara technique the same result can be obtained even more easily. At $T \rightarrow \infty$ all kernels of the spectral function λ_k , defined by Eq. (7), vanish as $1/(\langle \Omega_{boson}^2 \rangle + 4\pi^2 k^2 T^2)$ for all k , except $k=0$. Therefore, the Eq. (6) for the renormalized frequency becomes trivial

$$\tilde{\omega}_n = \omega_n + \gamma_{imp}/2 + \pi\lambda T. \quad (39)$$

If one substitutes the obtained $\tilde{\omega}(\omega)$ in Eq. (8) or $\tilde{\omega}(i\omega_n)$ into Eq. (9) after some algebra one arrives at the Drude type expression for the optical conductivity

$$\sigma(\omega) = \frac{\omega_{pl}^2}{4\pi} \frac{1}{\gamma_{imp} + 2\pi\lambda T - i\omega}. \quad (40)$$

Note, that the relation $\gamma_{opt} = 2\gamma_{eff} \equiv -2Im\Sigma$ is correct, if and only if the self energy $\Sigma(\omega) = \omega - \tilde{\omega}(\omega)$ does not depend on frequency. Otherwise, the relation

$$\gamma_{opt}(\omega) = -2Im\Sigma(\omega) \quad (41)$$

does not satisfy the Kramers-Kronig (K.-K.) relations, that is, it violates the causality. The proof is very simple. Due to the charge conservation law, when the photon has been absorbed, *two* quasiparticles, "the electron" and "the hole" come into being. The optical conductivity is a bosonic function defined by its values at ν_k , while the quasiparticle self energy $\Sigma(\omega)$ is a fermionic function defined by the values at ω_k . As a result, the right and left hand sides of Eq. (41) have different statistics, what is very

strange. In frame of the ISB model considered here the proof is a little bit more complicated. The optical conductivity itself and its inverse $1/\sigma(\omega)$ are response functions. It means, that they have no poles on the upper half-plane of the complex frequency or, in other words, their real and imaginary parts are connected by Kramers-Kronig relations. The same is valid for the self energy. From Eq. (41) after K.-K. transformation one obtains

$$m_{opt}^*(\omega) - 1 = 2(m_{eff}^*(\omega) - 1). \quad (42)$$

The optical and effective masses have the same asymptotic value $1+\lambda$ at $\omega, T \rightarrow 0$. Due to the presence of the factor of 2 in (42) it would mean, that $1=2$.

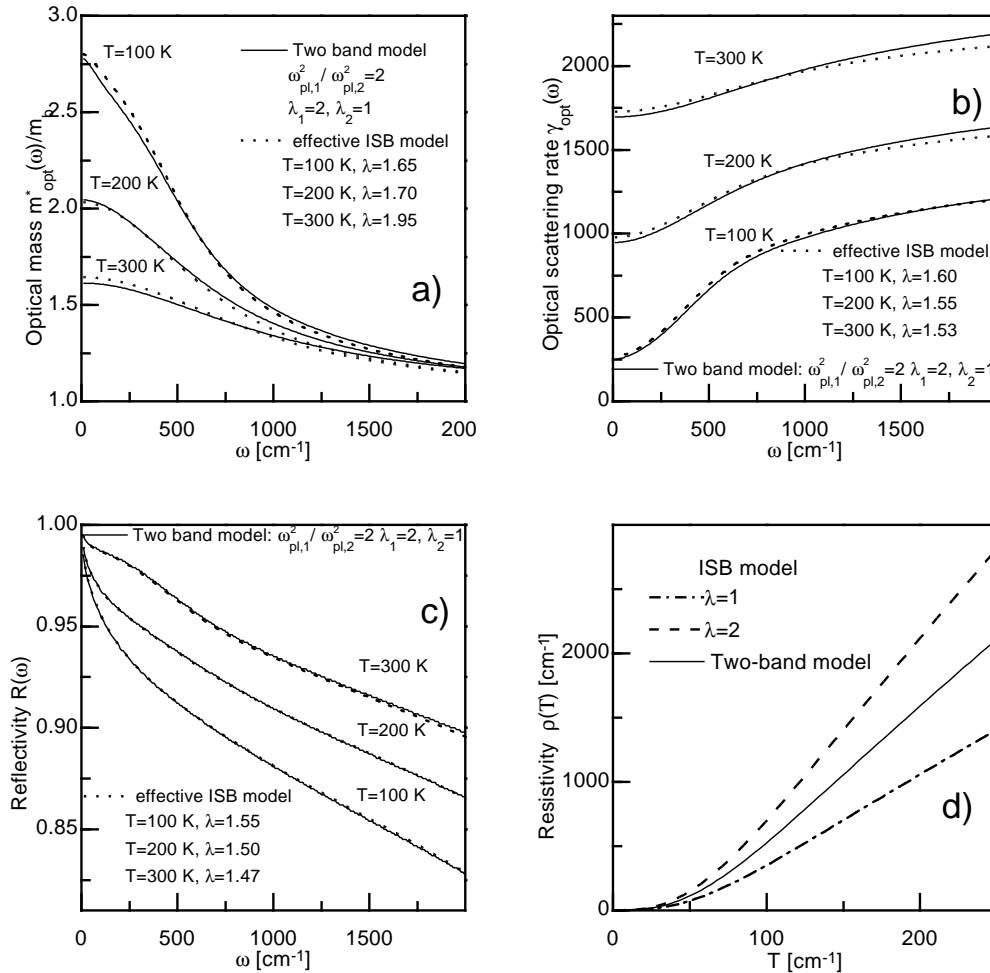


FIG. 5. The frequency and temperature dependencies of the two-band optical mass, scattering rate, reflectivity and DC resistivity are shown by solid lines in panels a, b, c, d respectively. The corresponding ISB fitted counterparts are plotted by the dotted lines.

Let us turn to the temperature dependence of the optical properties of ISB metals, which are shown in Fig. 4. All curves were calculated using model 2 spectral function and $\gamma_{imp} = 0$. Panel 4a presents the frequency dependence of the optical scattering rate $\gamma_{opt}(\omega, T)$ (solid lines) for $T=100$ K, 200 K, 300K. The corresponding optical masses are shown in panel 4b. One can see, that the absolute value of $\gamma_{opt}(\omega, T)$ increases with T , but the frequency dependent component decreases. It leads to diminishing of $m_{opt}^*(\omega, T)/m_b$ when T is rising. The temperature dependence of the minimum ($\omega = 0$, solid line) and maximum ($\omega = \infty$, solid line) values of $\gamma_{opt}(\omega)$ are shown in panel 4d in comparison with their common asymptote $\gamma = 2\pi\lambda T$ (dotted line). The corresponding function $m_{opt}^*(\omega = 0, T)/m_b$, named

sometimes $1 + \lambda_{opt}(T)$ is presented in panel 5c. The position of maximum of the small hump at low T is approximately equal to $\Omega_{min}/5$, where Ω_{min} is the frequency position of the lowest boson peak in $\alpha^2 F(\omega)$. At the same temperature the DC resistivity $\rho(T) = 4\pi\gamma_{opt}(\omega = 0, T)/\omega_{pl}^2$ starts the linear rise. In subsection II B the simple rule for determination of the *upper* frequency bound of the spectral function Ω_{max} was proposed. At $\omega \approx \Omega_{max}$ the optical mass without unity ($m_{opt}^*(\Omega_{max}, T)/m_b - 1$) is approximately the half of its value at $\omega = 0$. The temperature dependence of the quantity $\omega_{(m^*-1)/2}$ defined by

$$2[m_{opt}^*(\omega = \omega_{(m^*-1)/2}, T)/m_b - 1] = m_{opt}^*(\omega = 0, T)/m_b - 1 \quad (43)$$

is shown by solid line on inset in panel 4c in comparison with the phenomenological line $\omega = 5T$. One can see, that

$$\omega_{(m^*-1)/2} \approx max(5T, \Omega_{max}) \quad (44)$$

The normalised optical scattering $\gamma^*(\omega) = \gamma_{opt}(\omega)/m_{opt}^*(\omega, T)/m_b$ is shown in Fig(4a) (dotted lines). In our opinion [7] this quantity is far useless in comparison with $\gamma_{opt}(\omega)$ and $m_{opt}^*(\omega, T)/m_b$. With the exception of the low frequency region where its value is constant, $\gamma^*(\omega)$ is a quasilinear function $\propto \omega$ up to $max(4\Omega_{max}, 2\pi\lambda T)$. Even the simple analysis by the favourite polynom Eq. (33) allows to determine the four parameters, while $\gamma^*(\omega)$ depends on two. It is interesting, that the Gilbert transformation from $\gamma^*(\omega)$ is not equal to 0. In this connection we note that the use of the BSC normal state conductivity expression

$$\sigma(\omega) = \frac{\omega_{pl}^{*2}}{4\pi(\gamma^* - i\omega)}, \quad (45)$$

is correct, only if $\gamma^* = const$. Here $\omega_{pl}^{*2} = \omega_{pl}^2/(1 + \lambda)$ is the frequency-independent renormalised plasma frequency.

Note, that according to the Allen formula (31), the optical relaxation is approximately *linear* with respect to the spectral function $\alpha^2 F(\omega)$. It means, that the conversion from the low temperature scenario to the asymptotic high temperature one takes place for each boson with frequency Ω_i separately at $T \approx \Omega_i/5$, that is, when Ω_i becomes of the order of the *first* Matsubara energy $\nu_1 = 2\pi T$.

Since the isotropic single wide band model is the subject of the present lecture, discussing the properties of two-band systems we have to pay special attention to possible artefact results. Let us start our consideration from the temperature independent two-Drude terms simulator (36). Since it is equivalent to the favourite polynom (33), we can "extract the information about spectral function" including the temperature dependence of the coupling constant $\lambda(T)$. It is known, that if the material parameters are temperature independent, the optical scattering rate $\gamma_{opt}(\omega, T)$ is a monotonically increasing function. Since the simulator's $\gamma_{opt}(\omega)$ does not changes, when T is rising, one may conclude, that the coupling "constant" $\lambda(T)$ is a monotonically decreasing function with the high temperature asymptote $1/T$. On the other hand, the analysis of the optical mass, which is usually a monotonically decreasing function, gives the opposite result: $\lambda(T)$ dramatically increases when temperature is growing. The study of the reflectivity $R(\omega, T)$ gives the third fitted function $\lambda(T)$. The reasonable way to resolve this conflict is the replacement of the model. If one restricts oneself to the consideration of the scattering rate only, the contradiction can be overlooked. The fact is that the strong temperature dependence of material parameters exists, for example, in heavy fermion systems. Another interesting scenario was realised in fullerenes, where the DC resistivity (measured at the constant pressure) changes with temperature as T^2 and the same DC resistivity (measured at the constant volume) follows conventional linear law $\rho \propto T$, as it should be, since the theory assumes the $V=const$ condition.

The second example is the clean limit of anisotropic systems. As usually, one can divide the Fermi surface between two (for simplicity) parts with the approximately uniform properties. This disjointed representation of the Fermi surface is known as the multiband model. We accept also, that the intra- and interband interactions are governed by the electron-boson spectral functions having the same "model 2" shape, but different coupling constants λ_{ij} . The scales of transport and optical properties of the bands are fixed by the plasma frequencies $\hbar\omega_{pl,i}^2 = 4\pi e^2 v_{F,i}^2 N_i(0)/3$. In the normal state is possible to diagonalise the equations by the substitution $\lambda_1 = \lambda_{11} + \lambda_{12}$ and $\lambda_2 = \lambda_{21} + \lambda_{22}$. The resulting two-band optical conductivity is the sum of two ISB terms (8). For the model calculations the arbitrary values $\lambda_1 = 2$, $\lambda_2 = 1$ and $\omega_{pl,1}^2/\omega_{pl,2}^2=2$ was chosen.

The frequency and temperature dependencies of the two-band optical mass, scattering rate, reflectivity and DC resistivity are shown by solid lines in Fig. (5)a, b, c, d respectively. The *by-eye-analysis* can not reveal the difference between clean limit two-band optical properties and the standard ISB ones. Fortunately, the ISB model can pose several possibilities for a quantitative study. I simply fit the two-band curves, shown on panels (5)a, b, c, by the appropriate ISB ones (dotted lines), calculated using the same "model 2" spectral function. The coupling constant λ was used as fitting parameter. One can see, that the temperature dependencies of $m_{opt}^*(\omega, T)/m_b$, $\gamma_{opt}(\omega, T)$ and $R(\omega, T)$ of the anisotropic system are yet weaker, that it should be according to the ISB rules. The fitted functions $\lambda(T)$ grow or drop, when T is rising, depending on which quantity has been chosen for the fit.

For the few metals, where the mutual anisotropy of $\lambda(\mathbf{k})$ and of $v_F(\mathbf{k})$ was investigated, the following regularity was found. The quasiparticles with smaller $v_F(\mathbf{k})$ have larger $\lambda(\mathbf{k})$. Usually this information is unavailable. One can estimate the anisotropy, if one compares the material parameters obtained from the optical spectra with the ones revealed by the analysis of thermodynamic, or point-contact tunnelling data. The scale of the optical conductivity is fixed by $\omega_{pl}^2 \propto v_F^2 N(0)$. The normal state specific heat data are proportional to $(1 + \lambda)N(0)$. The point-contact tunnelling spectra are weighted by the factor v_F . As a result, if one treats optical spectra of anisotropic metals in terms of the ISB the model, one reveals the electron-boson coupling function $\alpha_{opt}^2 F(\omega)$, which distinguish itself by smaller value of the coupling function λ_{opt} in comparison with lambdas, obtained by other physical methods. This difference is usually assigned to the kinetic coefficient $(1 - \cos)$ [2] or, in another language, to the vertex corrections to the quasiparticle Green function [1]. It is interesting, that if the system under consideration is completely isotropic, and $\alpha^2 F(\omega, \mathbf{k}, \mathbf{k}')$ do not depend on \mathbf{k} and \mathbf{k}' , the vertex corrections vanish as soon as considered in this subsection usual anisotropy effects. What kind of corrections are more important in each particular case, first order vertex ones or discussed here zero order distortions caused by the interplay of $v_f(\mathbf{k})$ and $\lambda(\mathbf{k})$, it is the question for the gallop band structure calculations.

In conclusion, the temperature dependence of the optical properties of ISB metals really exists and can be well quantitatively described. It originates mainly from the presence of the Bose factor in Eqs.(5) (\equiv sampling in (6)) and to a lesser extent from the presence of the Fermi distributions in Eqs.(5-9). The principal deviation from the predicted frequency and temperature behaviour manifests that the chosen ISB model is not complete and has to be replaced.

E. Optical mass and scattering rate in mid-infrared: artefacts generated by overlooking of interband transitions and underestimation of ϵ_∞ .

The formal textbook relation between the conductivity $\sigma(\omega)$ and permeability $\epsilon(\omega)$

$$\epsilon(\omega) = 1 + \frac{4\pi i \sigma(\omega)}{\omega} \quad (46)$$

is not suitable for a practical use, since the entering Eq. (46) $\sigma(\omega)$ reflects the total response of all excitations.

The simplest reasonable decomposition of (46), valid over the spectral region up to frequencies just above plasma edge, is

$$\epsilon(\omega) = \epsilon_\infty + \epsilon_{inter}(\omega) + \epsilon_{phonon}(\omega) + \frac{4\pi i \sigma(\omega)}{\omega}, \quad (47)$$

where ϵ_{inter} and ϵ_{phonon} are the contributions of interband transition(s) and direct IR active phonons centred below plasma edge. The response of high energy excitations and wide interbands, overlapping the plasma edge is presented by the complex constant ϵ_∞ . $\sigma(\omega)$ is *the quasiparticle* conductivity, defined by Eqs.(8,10).

The direct phonon band contribution will not be considered, since it is usually weak and plays some role only in the selected compounds containing light elements and having small value of ω_{pl} , for example, in doped fullerenes.

The used here model interband contribution

$$\epsilon_{inter}(\omega) = \frac{\omega_{pl,inter}^2}{\Omega_0^2 - \omega^2 - i\omega\gamma_{inter}} \quad (48)$$

is the simple Lorentzian with $\omega_{pl,inter}=16000 \text{ cm}^{-1}$, $\Omega_0=4000 \text{ cm}^{-1}$, and $\gamma_{inter}=6000 \text{ cm}^{-1}$. The overlooking of the interband contribution was simulated as follows. The sum of two terms given by Eqs. (48) and (8) was treated as the quasiparticle response in terms of the optical mass and scattering rate

$$\gamma_{opt}(\omega, T) - i\omega m_{opt}^*(\omega, T)/m_b = \frac{\omega_{pl}^2 + \omega_{pl,inter}^2}{4\pi\sigma(\omega) - i\omega\epsilon_{inter}(\omega)}. \quad (49)$$

For simplicity I set $\omega_{pl} = \omega_{pl,inter}$ and following to

The results are shown in Figs. 6a, 6b and 6c by solid lines. The "true" masses and scattering rates

$$\gamma_{opt}(\omega, T) - i\omega m_{opt}^*(\omega, T)/m_b = \frac{\omega_{pl}^2}{4\pi\sigma(\omega)}. \quad (50)$$

and the *chi-by-eye* [19] fit by the formula (33) are plotted in Figs. 6a, 6b and 6c by dotted and dashed lines respectively.

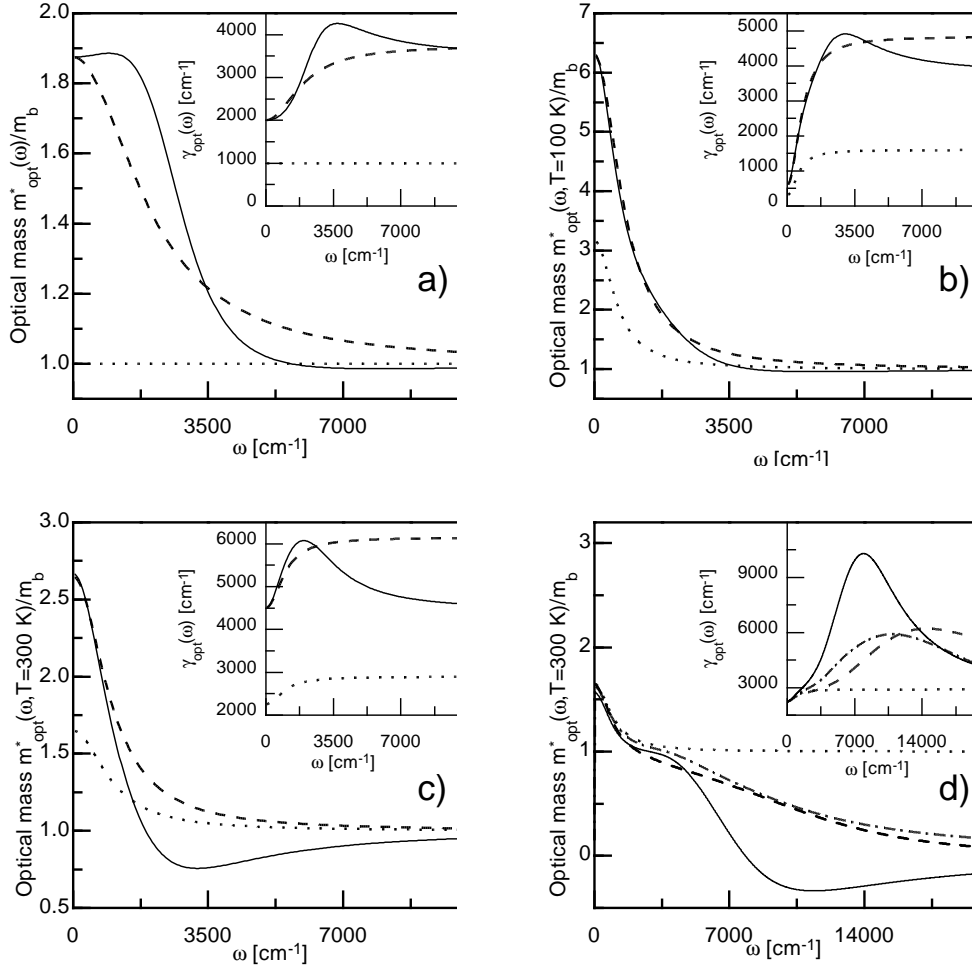


FIG. 6. The artefact frequency dependencies of the optical masses and scattering rates (insets) generated by the overlooking of interband transition (panels a, b, c) and the underestimation of ϵ_{∞} (panel d) are shown by solid lines. The true, unperturbed frequency dependencies of $m_{opt}^*(\omega)/m_b$ and $\gamma_{opt}(\omega)$ are plotted by dotted lines. The dashed lines in panels a, b, c are the *chi-by-eye* fitted curves (by Eq. 32). For parameters of the model interband transition and trial ISB quasiparticle optical conductivities see text.

Note, that due to the frequency averaging, the quasiparticle optical conductivity (8,10) is a slowly varying function in the mid-infrared region. In contrast, the interband permeability near transition edge

(here, near the center of the Lorentzian) can change rapidly. The second important feature of $\epsilon_{inter}(\omega)$ is its very weak temperature dependence.

The mixture of the standard Drude term ($\gamma=1000 \text{ cm}^{-1}$) with the Lorentzian (48) is shown in panel 6a. This simple artefact can be easily recovered, since it is temperature independent and the optical mass changes too quickly.

The second and third examples are the half-by-half blends of the "model 2" ISB conductivities (T=100 K, panel 6b; T=300 K, panel 6c) with the same $\epsilon_{inter}(\omega)$ Eq. (48). It is more complicated case, since the nonmonotonic behaviour could be screened by forthcoming transitions. In this case detailed quantitative analysis of both the frequency and the temperature dependencies is needed. One has to pay the special attention to the temperature dependencies of $m_{opt}^*(\omega \rightarrow 0, T)/m_b$, $\omega_{(m^*-1)/2}$ and $\gamma_{opt}(\omega \approx 2\pi\lambda T, T)$.

If the interband transitions are wide spectral bands without unqualified features, their contribution to the permeability is usually included in ϵ_∞ . The effects caused by the underestimation of its real part was considered by us in [7]. Here we study the problems produced by the use of Eq. 46 and by the underestimation of the imaginary part of ϵ_∞ . Since the last quantity can be approximated by the simple constant only in the limited frequency range, for the sake of the analytical correct the model function was chosen in the form

$$\begin{aligned} Im(\delta\epsilon_\infty(\omega)) &= \left[\tanh\left(\frac{\omega - 2000}{5000}\right) + \tanh\left(\frac{50000 - \omega}{30000}\right) \right] \quad \text{at } \omega > 0, \\ Im(\delta\epsilon_\infty(-\omega)) &= -Im(\delta\epsilon_\infty(\omega)), \\ Im(\delta\epsilon_\infty(0)) &= 0, \\ Re(\delta\epsilon_\infty(\omega)) &= 2.5 - \frac{2\omega}{\pi} \int_0^\infty \frac{dx Im(\delta\epsilon_\infty(x))}{x^2 - \omega^2}. \end{aligned} \quad (51)$$

In the mid infrared ($\delta\epsilon_\infty(\omega) \approx 4 + 2i$).

The model frequency dependencies of the optical masses and scattering rates

$$\gamma_{opt}(\omega, T) - i\omega m_{opt}^*(\omega, T)/m_b = \frac{\omega_{pl}^2}{4\pi\sigma(\omega) - i\omega\tilde{\delta}(\epsilon_\infty)}. \quad (52)$$

are shown in panel 6d for $\tilde{\delta}(\epsilon_\infty) = \delta(\epsilon_\infty(\omega)) - 1$ (solid lines), $\tilde{\delta}(\epsilon_\infty) = \delta(\epsilon_\infty(\omega)) - 4$ (dashed-dotted lines), and $\tilde{\delta}(\epsilon_\infty) = 2i$ (dashed lines). The unperturbed $\gamma_{opt}(\omega, T)$ and $m_{opt}^*(\omega, T)/m_b$ ("model 2" spectral function, $\lambda=2$, T=300 K) are plotted by dotted lines for comparison. As usually, the masses do not lie, and manifest that the "unusual" frequency dependence of the scattering rate is no more than the artefact of the chosen interpretation procedure.

The early band structure calculations [27] predicted, that the interband contribution into the in-plane HTSC permeability is a real constant between 10 and 15 at $\omega \rightarrow 0$, and becomes complex for $\omega > 0.4eV$. In the vicinity of the plasma edge its value is $4+2i$. This information was used by us for the successful description of the *normal state* optical properties of HTSC materials both in FIR and MIR spectral regions [7,15].

In conclusion, the overlooked interband transitions produces the "unusual" frequency dependence of the optical relaxation, which can be nevertheless analysed properly within the ISB model.

F. Why is the first derivative from the experimental curve better than the second one?

Let us rewrite the valid at T=0 Eqs.(29,30) in the differential form

$$\alpha^2 F(\omega) = \frac{1}{2\pi} \frac{d\gamma_{eff}(\omega)}{d\omega} \quad (53)$$

$$\alpha^2 F(\omega) = \frac{1}{2\pi} \frac{d^2(\omega\gamma_{opt}(\omega))}{d\omega^2}. \quad (54)$$

At a glance both Eqs. (53) and (54) look nice and simple. But if one attempts to apply them to an experimental data, the distinction becomes evident. The point is that the experimental data are known only approximately. A finite value of the signal to noise ratio (S/N) is the reason why the Eq. (54)

can not be applied to the FIR data. Typical value of the reflectivity S/N do not exceed 50, the multi-reflection techniques [3] allow to reach S/N=2000. Let us adopt for simplicity, that $f(\omega) = \omega\gamma_{opt}(\omega)$ is sampled in equidistant points ω_i , $i = 1, M$ and all values $f(\omega_i)$ have the same errors

$$\frac{f(\omega_i)}{\delta f(\omega_i)} = \left(\frac{S}{N}\right)_f. \quad (55)$$

Note, that in the normal state at $T = 0$ (when the application of (53) and (54) is correct) both $f(\omega) = \omega\gamma_{opt}(\omega)$ and its first derivative $f'(\omega)$ are monotonically increasing functions, if a metal under consideration is the ISB one.

The difference $f(\omega_{i+1}) - f(\omega_i)$ has the order of $f(\omega_i)/M$. Its error is the $\sqrt{\delta f^2(\omega_{i+1}) + \delta f^2(\omega_i)} \approx \sqrt{2}\delta f(\omega_i)$. As a result the first derivative $f'(\omega)$ has the signal to noise ratio

$$\left(\frac{S}{N}\right)_{f'} = \frac{f'(\omega_i)}{\delta f'(\omega_i)} = \frac{f(\omega_{i+1}) - f(\omega_i)}{\sqrt{\delta f^2(\omega_{i+1}) + \delta f^2(\omega_i)}} \approx \frac{1}{\sqrt{2}M} \left(\frac{S}{N}\right)_f, \quad (56)$$

reduced by the factor $K_1 = \sqrt{2}M$ in comparison with the original (S/N) in $f(\omega)$. Similar the second derivative $f''(\omega)$ has the signal to noise ratio

$$\left(\frac{S}{N}\right)_{f''} = \frac{f''(\omega_i)}{\delta f''(\omega_i)} = \frac{(f'(\omega_{i+1}) - f'(\omega_i))'}{\sqrt{\delta f'^2(\omega_{i+1}) + \delta f'^2(\omega_i)}} \approx \frac{1}{2M^2} \left(\frac{S}{N}\right)_f, \quad (57)$$

reduced by the factor $K_2 = 2M^2$.

In subsection II C the four parameters formula (33) was promoted as the universal fitting tool. $M = 4$ means $K_2 = 32$. In another words, the normal state $\gamma_{opt}(\omega)$ has to have the original signal to noise ratio (S/N)=100, in order to define *four* points in its second derivative $\gamma''_{opt}(\omega)$ with accuracy of 30%.

As for K_1 , this quantity grows reasonably. Of course, one can not measure the effective scattering rate $\gamma_{eff}(\omega)$ and use the formula (53), nevertheless the title question is worth-while. The point is that the first derivatives from the superconducting state optical scattering rate $\gamma'^s_{opt}(\omega)$ and the reflectivity $R'(\omega)$ reproduce the input spectral function $\alpha^2 F(\omega)$ [2,3,20,21]. The well structured spectral function of lead obtained from the analysis of the first derivative of $A_s(\omega) - A_n(\omega)$ looks convincing (at least for me) due to the reported value of S/N=6000.

Analysing Eq. (54) we arrive at the same conclusions as discussed above. The normal state optical conductivity provides us with restricted information similarly as other physical methods. The only way to extract the all required material parameters values is the analysis of different measurements in frame of the *same* model.

III. SUPERCONDUCTING STATE OPTICAL CONDUCTIVITY

A. The inversion procedure

1. Adaptivity, what does it mean?

Let us consider from a general point of view the problems, which one has to take in mind, when one try to reconstruct a spectral function $\alpha^2 F(\omega)$ from experimental reflectivity data. This analysis should be performed in frame of a model which is based on an appropriate formalism. Thus, it means, that the results obtained are model dependent. The ideal, but rare situation occur, when the exact analytical solution of the inverse problem is available

$$\alpha^2 F(\omega) = f(R(\omega), \omega) \quad (58)$$

where f is a known function, which could depend on $\alpha^2 F(\omega)$. In the last case the numerical solution can be found by iterations.

But what should we do, if such a function f is not available by reason of the complexity of the direct formalism. In this case we shell use the numerical *adaptive strategy*, based on the substitution

of equations of the direct formalism by the *adaptive* formula(s), suitable for the numerical solution of ill-posed problems. Since it is a strategy, let us consider how does the adaptivity work.

Generally speaking, one can use *any* adaptive formula. For example, one can consider the $\alpha^2 F(\omega)$ as an input function and the reflectivity as an output function for some formalism. Then one could write

$$R(\omega) = \int dz K(\omega - z) \alpha^2 F(z), \quad (59)$$

or in the Fourier space

$$\mathcal{F}(R(x)) = \mathcal{F}(K(x)) \mathcal{F}(\alpha^2 F(x)), \quad (60)$$

where $\mathcal{F}(f(x))$ is the Fourier image of the function f and $K(x)$ is an for the time being unknown kernel. $K(x)$ could be determined as follows.

- At first, one has to substitute a *trial* spectral function $\alpha_{trial}^2 F(\omega)$ into the equations of the main formalism (Eliashberg equations + Nam-Rainer formula) and obtains a *trial* reflectivity $R_{trial}(\omega)$.
- Next, one should substitute $\alpha_{trial}^2 F(\omega)$ and the *calculated* $R_{trial}(\omega)$ into the adaptive formula (60) and solve Eq. (60) for $K_1(\omega)$. The subscript 1 means "the first iteration".
- Finally, one has to substitute the *now known* kernel $K_1(\omega)$ and the *experimental* $R_{exp}(\omega)$ into the same adaptive formula (60), and solve it for $\alpha_1^2 F(\omega)$.

So, on each iteration we use the model formalism ones and the adaptive formula twice. At first, one have to calculate $R_{k-1}(\omega)$ using $\alpha_{k-1}^2 F(\omega)$, as input function. At second, one should find the adaptive function(s)

$$\mathcal{F}(K_k(x)) = \frac{\mathcal{F}(R_{k-1}(x))}{\mathcal{F}(\alpha_{k-1}^2 F(x))}, \quad (61)$$

and finally calculate the spectral function

$$\mathcal{F}(\alpha_k^2 F(x)) = \frac{\mathcal{F}(R_{exp}(x))}{\mathcal{F}(K_k(x))}. \quad (62)$$

The presented "trick" is quite general. One could replace analogously, for example, $R(\omega)$ in (59-62) by the tunnelling density of states $N(\omega)$ or the ARPES spectral function $A(\omega)$, and obtain adaptive methods for the tunnelling and electronic spectroscopies respectively, which is expected can work, with any formalism.

As mentioned above, the experimental data are known only approximately, therefore the inverse problem is ill-posed. Up to now the solution of ill-conditioned problems is the art more than the routine procedure. Since one can use any adaptive formula(s), it will be pragmatic for him/her/AI to choose it from the short (alas!) list of well investigated by numerical mathematics equations (see, for example, sec. 18.4-18.7 in [19] and references within).

On this understanding the discussed above convolution adaptive formula is one of the best possible selections, since the Fourier transformation is linear and unitary.

2. The inversion method for the s-wave ISB reflectivity.

The inverse problem for the superconducting state optical absorptivity of Pb was successfully solved by B. Farnworth and T. Timusk [3] within the weak coupling ISB model, based on the theory proposed by P.B. Allen [2]. The difference between weak coupling theoretical calculations and experimental data [20] was analysed in detail in [2]. It was pointed, that:

- The first derivative from the superconducting state optical scattering rate contains the component, proportional to the input spectral function $\alpha^2 F(\omega)$ due to the influence of coherent factors (11).
- The weight $\omega/2\Delta_0$ of this component is strongly underestimated.

- If one substitutes the solutions of (2) into the dominators of (10) and keeps BSC values $\tilde{\omega} = \omega$ and $\tilde{\Delta} = \Delta_0$ for the coherent factors (11), one obtains the optical relaxation, close to the one, given by the weak coupling Allen theory.

Below we will see that ISB model based on the Nam formalism have qualitatively the same properties. There are several reasons, why the following convolution adaptive formula

$$\frac{\gamma_{opt}^s(\omega)}{d\omega}\theta(\omega) = 2\pi \int dz K(\omega - z)\alpha^2 F(z)\theta(z) \quad (63)$$

$$\theta(x) = 1 \text{ if } x \geq 0, \text{ else } \theta(x) = 0$$

is suitable. At first, we segregate the ill-posed part of the inverse s -wave problem (taking of the first derivative) into the separate step. At second, the low and high frequency values of $\gamma_{opt}^s(\omega)$ coincide ($=0$), it is important for the FFT algorithm. At third, the obtained kernel $K(\omega)$ reminds us the instrumental resolution function of a badly adjusted spectrometer, allowing to profit by the applied spectroscopy experience. If one thinks in terms of the transfer functions, Laplace transformation adaptive formula could be more suitable.

The equation (63) was solved with respect to $K(\omega)$ using optical scattering rates *calculated* in strong (solid line, Fig. 7b) and weak (dashed line, Fig. 7b) coupling approximations and input "model 2" $\alpha^2 F(\omega)$. The results are plotted by the same type lines in Fig. 7a. No doubt, all features of the kernel are important for the recovery of the precise peak amplitudes and energy positions. Nevertheless, the general shape and main physics of $\gamma_{opt}^s(\omega)$ are defined by the *master* peak, located just above $\omega = 2\Delta_0$. The arrow, pointing in Fig. 7a the frequency position of $2\Delta_0$, is located within this peak. The master peak income is illustrated by dotted line in Fig. 7b. It was calculated as follows.

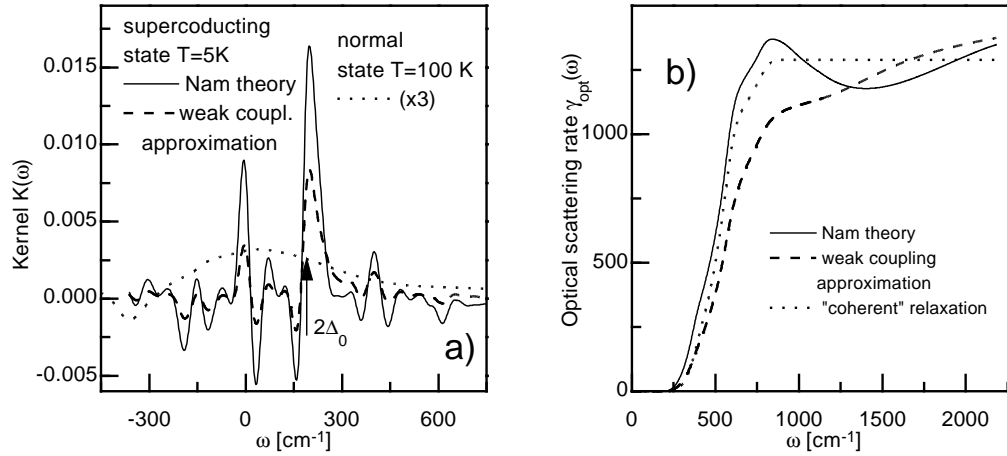


FIG. 7. Panel (a) shows the frequency dependence of the superconducting state kernels $K(\omega)$ (solid and dashed lines) in comparison with the normal state one (dotted line). The source superconducting state optical scattering rates, calculated in the strong (solid line), and weak (dashed line) coupling approximations are shown in panel (b). The convolution of the input spectral function with the master peak (="coherent" relaxation) is drawn in panel (b) by the dotted line.

- All collateral maxima and minima of the shown by solid line $K(\omega)$ were rejected and artificial kernel $K_{coh}(\omega)$ was set to zero anywhere besides the master peak frequency region, where it coincides with $K(\omega)$.
- $K_{coh}(\omega)$ was convoluted with the input spectral function $\alpha^2 F(\omega)$ and integrated over ω
- Since the discussed phenomenon is governed by the coherence factors, the resulting "scattering rate" (dotted line, Fig. 7b) is labelled as *coherent relaxation*.

- The simple frequency dependence of the coherent relaxation, reminding us the properties of the quasiparticle effective scattering rate $\gamma_{eff}(\omega)$, allow to enunciate the Visual Accessibility procedure, described in forthcoming section.

The normal state kernel (multiplied on 3) is shown by the dotted line on Fig. 7a for comparison. The pessimistic conclusion, made in the previous chapter, can be couched in current terms: the (induced by the frequency and temperature averaging) width of $K(\omega)$ is too large to resolve the fine structure of the spectral function.

The domination of the master peak makes the choice of the trial $\alpha^2 F(\omega)$ on the first iteration easy. It can be the normalised $\gamma'_{opt}(\omega)$ or $R'_s(\omega)$. Note, that the master peak is asymmetric. The final frequency resolution is defined by the small value of its left half-width.

The self-consistent determination of the value of the superconducting gap is theoretically possible in frame of adaptive approach, but strongly not recommended. Following this way one transforms the weakly nonlinear task to the strongly nonlinear problem. For the case of ill-conditioned equations it is the wrong way. The value of Δ_0 has to be known *a priori*. The related issue is the difference between $\alpha^2 F(\omega)$ and $\alpha_{tr}^2 F(\omega)$. Substituted to the Eliashberg equations transport spectral function $\alpha_{tr}^2 F(\omega)$ lands us in difficulty, since the obtained value of the gap can be lower than the known Δ_0 . In my opinion, for the sake of simplicity in this case one might sacrifice the unknown (from the first principle calculations) Coulomb pseudopotential and use μ^* as a simple fitting parameter.

In conclusion, the *adaptive* method of the *exact numerical inversion* of the s-wave superconducting state Nam equations is presented. In my opinion, one day the FIR spectroscopy will provide not an alternative to the tunnelling, but a powerful independent tool for the determination of $\alpha^2 F(\omega)$ in s-wave superconductors.

B. Rules of Visual Accessibility procedure

The frequency dependence of the superconducting state ISB reflectivity $R_s(\omega)$ in the local limit has the distinctive forms. This features are determined by the physical properties of the optical scattering rate $\gamma_{opt}^s(\omega)$. In this section we consider our simplified approach (Visual Accessibility) which allow us to analyse "by eye" the experimental reflectivity curve and get qualitatively the same results as the sophisticated method, described in the previous section, able to obtain quantitatively.

1. Optical scattering rate and reflectivity

As far as the physics is determined by the $\gamma_{opt}(\omega)$, but the measured quantity is $R(\omega)$, let us derive a simple relation between them. In view of a high value of the permeability $\epsilon(\omega) \gg 1$ one can expand the formula

$$R(\omega) = \left| \frac{1 - \sqrt{\epsilon(\omega)}}{1 + \sqrt{\epsilon(\omega)}} \right|^2 \quad (64)$$

in powers of $1/\sqrt{\epsilon(\omega)}$. In view of Eq. (22), substituting $1 + \lambda$ instead of m_{opt}^*/m_b , one arrives the following approximate relation

$$R(\omega) \approx 1 - \frac{2\gamma_{opt}(\omega)}{\omega_{pl}\sqrt{1 + \lambda}} \quad (65)$$

valid at $\omega \leq \Omega_{max} + 2\Delta$ both in the normal ($\Delta=0$) and superconducting ($\Delta=\Delta_0$) states, except for small frequencies $\omega < \gamma_{opt}(0)/(1 + \lambda)$, where Hagen-Rubens approximation is suitable.

Fig. 8a shows the frequency dependence of the superconducting state reflectivity $R_s(\omega)$ (T=10 K, solid line) in comparison with the normal state reflectivity $R_n(\omega)$ (T=100K, dashed line). Both curves have been calculated using the "model 2" spectral function. The frequency dependencies of the optical scattering rates $\gamma_{opt}^s(\omega)$ and $\gamma_{opt}^n(\omega)$ are shown in the inset. One observes that $R(\omega)$ looks like the mirror image of the appropriate $\gamma_{opt}(\omega)$, reproducing all important features.

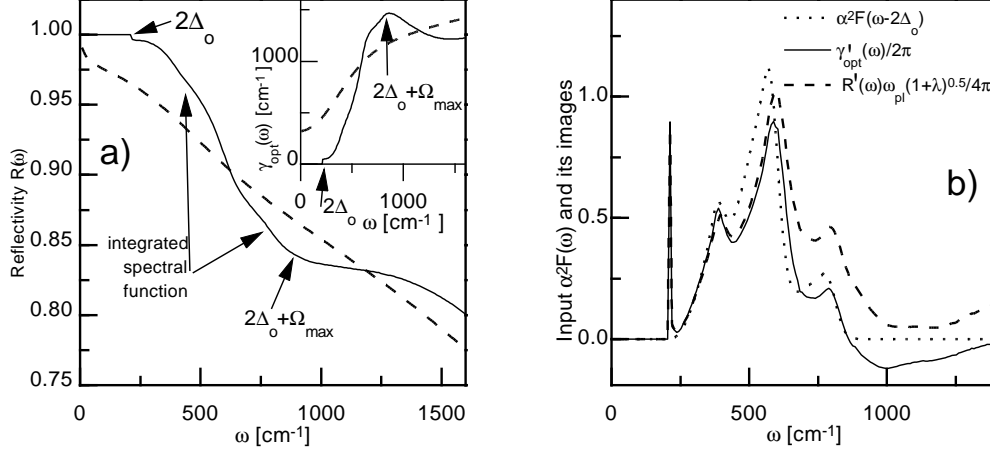


FIG. 8. Panel (a) shows the frequency dependence of the superconducting state reflectivity $R_s(\omega)$ ($T=10$ K, solid line) in comparison with the normal state reflectivity $R_n(\omega)$ ($T=100$ K, dashed line). Both curves were calculated using "model 2" spectral function. The frequency dependencies of the optical scattering rates $\gamma_{opt}^s(\omega)$ and $\gamma_{opt}^n(\omega)$ are shown in the inset. Panel (b) shows the frequency dependencies of the first derivatives from the optical scattering rate $\gamma_{opt}^s(\omega)/2\pi$ and from the normalised reflectivity $R'(\omega)\omega_{pl}(1+\lambda_0)^{0.5}/4\pi$ in comparison with the shifted $2\Delta_0$ input spectral function $\alpha^2 F(\omega - 2\Delta_0)$. One can see, that due to domination of the coherent relaxation in the frequency region between $2\Delta_0$ and $2\Delta_0 + \Omega_{max}$, $R'(\omega)\omega_{pl}(1+\lambda_0)^{0.5}/4\pi$ and $\gamma_{opt}^s(\omega)/2\pi$ reproduces well the peaks of the spectral function. The important features are indicated in panel (a). One can see, that the absorption onset at $2\Delta_0$, the frequency dependence of the coherent relaxation between $2\Delta_0$ and $2\Delta_0 + \Omega_{max}$, and its upper energy bound at $2\Delta_0 + \Omega_{max}$ are visually accessible. The term "integrated spectral function" means, that the first derivative over ω from this part of the spectrum reproduces $\alpha^2 F(\omega - 2\Delta_0)$.

2. The visual accessibility criteria for *s*-wave superconductors

Let us summarise our knowledge about the *s*-wave superconducting state optical relaxation rate and the local (London) limit reflectivity (see Fig. 8). The following features are visually accessible.

- The doubled gap value $2\Delta_0$ coincides with the absorption edge. If the $\omega < 2\Delta_0$, the reflectivity $R(\omega)=1$ and $\gamma_{opt}^s(\omega)=0$.
- The impurity scattering gives a sharp decrease of the reflectivity just above $2\Delta_0$. The magnitude of the "jump" is proportional to γ_{imp} . $\gamma_{opt}^s(\omega)$ jumps approaching γ_{imp} from above.
- In superconducting state the coherent relaxation dominates. Hence, the first derivatives from $\gamma_{opt}^s(\omega)$ and from $R(\omega)$ reproduce the shape of the spectral function (see Fig. 8b).
- Since the frequency dependence of the coherent relaxation rate grows faster, than the frequency averaged normal state one, and is fulfilled its maximum value at the frequency $\omega = 2\Delta_0 + \Omega_{max}$, at this point the ratio of the $\gamma_{opt}^s(\omega)/\gamma_{opt}^n(\omega)$ has a maximum, while the reflectivity ratio $R_s(\omega)/R_n(\omega)$ exhibits a minimum.

C. Visual accessibility and separable *d*-wave model

In this section we consider briefly, how the procedure described in section III B 2 should be corrected in order to make the main features of the *d*-wave ISB reflectivity visually accessible.

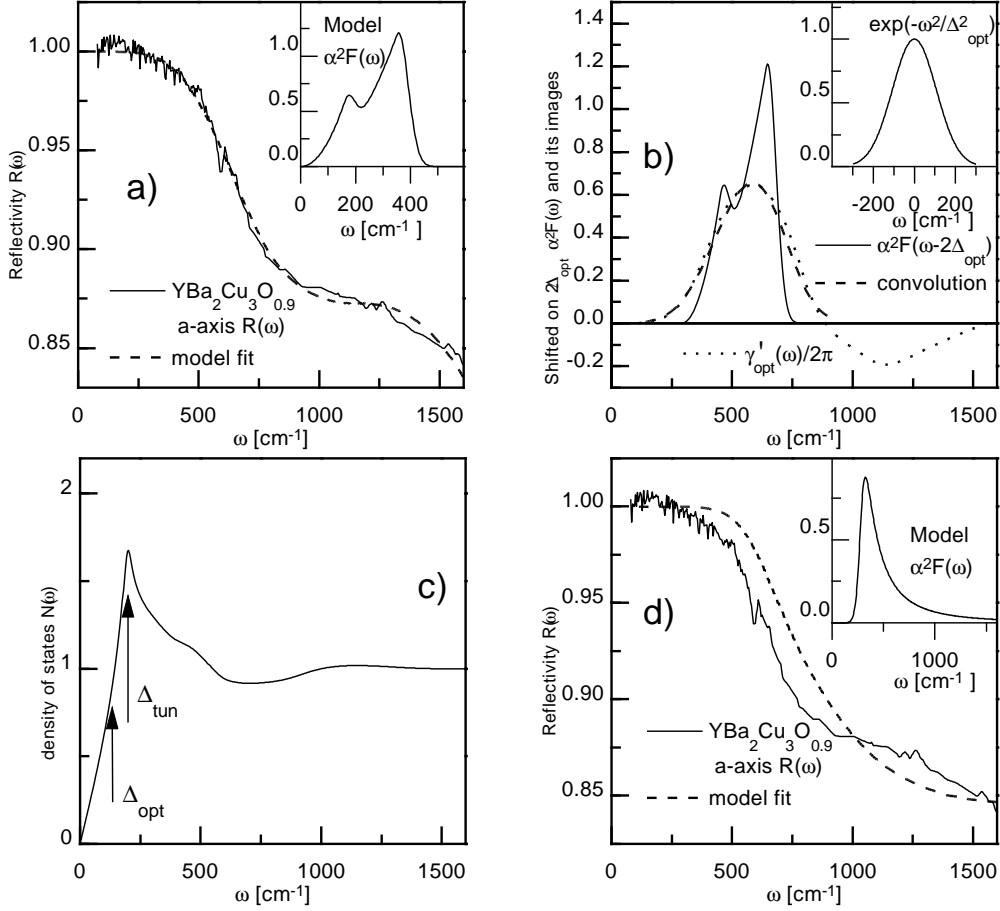


FIG. 9. Panels (a) shows the frequency dependency of the reflectivity $R_s(\omega)$ (dashed lines) calculated within the separable d -wave model in comparison with the experimental data (solid line, Schutzmann *et al Phys. Rev. B* **46** 512 (1992)). The spectral functions $\alpha_0 F(\omega)$ are shown in the insets. The coupling constants were chosen to obtain the value of the tunnelling gap $\Delta_{tun}=200$ cm $^{-1}$. The values of the plasma frequencies ω_{pl} and the low-frequency values of the non-metallic part of dielectric permeability ϵ_∞ were obtained by the least-square fit. Panel (b) shows the frequency dependence of the first derivative from the calculated optical scattering rate $\gamma_{opt}'(\omega)$ (dotted line) in comparison with the shifted on $2\Delta_{opt}$ input spectral function $\alpha_0^2 F(\omega - 2\Delta_{opt})$ (solid line). The convolution of the $\alpha_0^2 F(\omega - 2\Delta_{opt})$ with the Gauss distribution function (shown in inset (b)) is plotted by the dashed line. Panel (c) shows the frequency dependence of the calculated tunnelling density of states $N(\omega)$, the frequency positions of the tunnelling gap Δ_{tun} and the optical gap Δ_{opt} . Panel (d) shows the frequency dependencies of the reflectivity $R_s(\omega)$ (dashed lines), calculated using caudate spectral function (inset), in comparison with the experimental data.

Formally speaking, the frequency dependencies of the isotropic and the anisotropic parts of the spectral function are not obliged to coincide. At the same time, if the shapes differ substantially, the density of states (67) looks strange. So, for the sake of tunnelling, the model spectral function was chosen in the simple form

$$\alpha^2 F(\omega, \varphi) = \alpha_0^2 F(\omega)(1 + 2g \cos(2\varphi) \cos(\varphi')) \quad (66)$$

If one substitutes the function (66) into the $s + id$ ISB Eliashberg equations, one finds that at $g > 1$ the d -wave component entirely dominates. Hence, instead of the sophisticated $s + id$ approach, we can use

for our analysis the pure d -wave model described in detail in [31]. For the sake of simplicity we restrict ourselves here to the consideration of the clean limit $\gamma_{imp} = 0$ and set the Coulomb pseudopotential $\mu^*(\varphi, \varphi')$ to zero. The value of the parameter g was chosen little a bit larger than unity, since the normal state properties (defined in frame of *this* model by $\alpha_0^2 F(\omega)$) manifest the strong renormalization due to the phonon-electron interaction.

It is interesting, that it is possible after minor rehash to use the available s -wave computational programs for the strong coupling d -wave calculations. The clean limit version of the separable d -wave model keeps the convolution structure of the set (2). One has to substitute the angle averaged density of states

$$\left\langle \frac{\tilde{\omega}(y)}{\sqrt{\tilde{\omega}(y)^2 - \tilde{\Delta}^2(y)}} \right\rangle_{\varphi} = \frac{1}{\pi} \int_0^{\pi} \frac{\tilde{\omega}(y) d\varphi}{\sqrt{\tilde{\omega}^2(y) - 2\tilde{\Delta}^2(y)\cos^2(2\varphi)}} \quad (67)$$

instead of $N(\omega)$ (3) in (2), and the angle averaged density of pairs

$$\left\langle \frac{\tilde{\Delta}(y)}{\sqrt{\tilde{\omega}(y)^2 - \tilde{\Delta}^2(y)}} \right\rangle_{\varphi} = \frac{1}{\pi} \int_0^{\pi} \frac{2\tilde{\Delta}(y)\cos^2(2\varphi) d\varphi}{\sqrt{\tilde{\omega}^2(y) - 2\tilde{\Delta}^2(y)\cos^2(2\varphi)}} \quad (68)$$

instead of $D(\omega)$ (4) in (2). Similarly, the conductivity can be calculated using the Nam formula (10). For this purpose one should substitute $\Delta_d(x) = \sqrt{2}\Delta(x)\cos(2\varphi)$ instead of the $\Delta_s(\omega)$ into the element of integration in (10) and averages the obtained $\sigma(\omega, \varphi)$ over the angle φ .

Fig. 9a shows the model reflectivity $R_s(\omega)$, calculated in the frame of the separable d -wave model (dashed line) in comparison with the experimental data [5] (solid line). The spectral function $\alpha_0 F(\omega)$ is shown in the inset in Fig. 9(a), its coupling constant λ was chosen to reproduce the value of the *tunnelling* gap $\Delta_{tun} = 200 \text{ cm}^{-1}$ derived from the tunnelling spectra [32]. Note, that it was the same "model 2" [7] curve, used above, but without any high energy peak. The value of the plasma frequency ω_{pl} and low frequency value of the non-metallic part of dielectric permeability ϵ_{∞} were obtained by the least-square fit.

Fig. 9b shows the first derivative from the d -wave optical scattering rate $\gamma'_{opt}(\omega)$ (dotted line) in comparison with the shifted on $2\Delta_{opt}$ input spectral function $\alpha_0^2 F(\omega - 2\Delta_{opt})$ (solid line). Here we define the *optical* gap $\Delta_{opt} \approx \Delta_{tun}/\sqrt{2}$ as the physical quantity, with defines the shift of the spectral function $\alpha_0^2 F(\omega)$ in FIR and tunnelling spectroscopy. The distinction between Δ_{opt} and Δ_{tun} arises due to the angle averaging ($\langle \dots \rangle_{\varphi}$) both in the Eliashberg equations and in the conductivity calculation. The tunnelling gap Δ_{tun} (see Fig. 9c) is the maximum value of the d -wave gap

$$\Delta^d(\varphi) = \sqrt{2}\Delta\cos(2\varphi) \quad (69)$$

and the optical one is its mean square angle average. Note, that the dip in the density of states $N(\omega)$ (see Fig. 9c) arises at $\Delta_{opt} + \Omega_{max}$ and the electron-boson region starts in $N(\omega)$ at $\Delta_{opt} < \Delta_{tun}$. It means, that the low-energy excitations (if they contribute to the spectral function) will degrade the sharp peak in the tunnelling density of states.

If one substitutes $\gamma'_{opt}(\omega)$ in Eq. 63, one finds that coherent relaxation still dominates, but the main peak is substantially wider and can be approximated by a Gaussian function $Q \exp(-\omega^2/\Delta_{opt}^2)$ ((Fig. 9b, inset). The function

$$C(\omega) = \alpha_0^2 F(\omega - 2\Delta_{opt}) \otimes \frac{1}{\sqrt{\pi}\Delta_{opt}} \exp\left(-\frac{\omega^2}{\Delta_{opt}^2}\right) \quad (70)$$

is plotted by the dashed line in the Fig. 9b and agrees well with the $\gamma'_{opt}(\omega)/2\pi$. Here \otimes means a convolution. Note, that the coincidence of the prefactor Q with the $1/\sqrt{\pi}\Delta_{opt}$ is come-by-chance.

In my opinion, the additional ill-posed step, the *real* deconvolution of the Gaussian can not be performed using the data with reasonable value of (S/N), since the spectral function in these compounds have half-width of the order of Δ_{opt} . On the other side, if one (by chance) will find that $\gamma'_{opt}(\omega)$ or $R'(\omega)$ are structured, it means, that the ISB separable d -wave model is not suitable for HTSC and have to be replaced.

Strictly speaking, the d -wave reflectivity is less than unity at any frequency. At the same time, there is an onset of the absorption at some ω_Δ , where $R(\omega)$ becomes visually different from unity. Since the convolution $C(\omega)$ is wider than the input spectral function $\alpha_0^2 F(\omega)$, the position of the onset $\omega_\Delta < 2\Delta_{opt}$. For the model spectral function shown in the inset in Fig. 9a $\omega_\Delta \approx 1.4\Delta_{opt} \approx \Delta_{tun}$. Generally speaking, the selected boson modes could be responsible for the d -wave pairing. In this case the position of the absorption onset will be between $\Omega_{min} + \Delta_{opt}$ and $\Omega_{min} + \Delta_{tun}$, where Ω_{min} is the low frequency bound of the electron-boson interaction function. Similarly, the point where the coherent relaxation rate reaches its maximum, will be shifted by Δ_{opt} towards the high frequencies in comparison with its position in the s -wave superconductors. As a result, the reflectivity ratio $R_s(\omega)/R_n(\omega)$ exhibits a minimum and the scattering rate ratio $\gamma_{opt}^s(\omega)/\gamma_{opt}^n(\omega)$ has a maximum approximately at $\Omega_{max} + 2\Delta_{tun}$.

2. The visual accessibility criteria for d -wave superconductors

In ISB s -wave metals at the same frequency $\omega = \Delta_0$ the density of states exhibits three important features. At first, in this point $N(\omega)$ has a maximum. At second, since the averaged over \mathbf{k} value of Δ_0 coincides in this case with itself, the density of states at $\omega = \Delta_0$ changes most rapidly. At third, for $\omega < \Delta_0$, the value of $N(\omega)$ is equal to zero. In d -wave superconductors this structural feature has a different energy position. One could denote

- the position of the maximum in the density of states Δ_{tun} as the *tunnelling* gap;
- the value of the shift $2\Delta_{opt}$ of the image of the spectral function in the first derivative from the optical relaxation rate $\gamma'_{opt}(\omega)$ as the *optical* gap ,
- the frequency ω_Δ where $R_s(\omega)$ becomes visually distinct from unity as the onset of the absorption or as the *absorption* gap.

The approximate relations between the gaps are $\Delta_{tun} \approx \omega_\Delta \approx \sqrt{2}\Delta_{opt}$. Similar to the description of the visually accessible features made in subsection III B 2 for a s -wave metals, we can write the same criteria for the separable d -wave model. Note, that in comparison with the s -wave case, all presented below itemised statements are valid approximately only.

- The single gap value Δ_{tun} coincides with the absorption edge. If the $\omega < \Delta_{tun}$, the reflectivity $R(\omega) \approx 1$ and $\gamma_{opt}^s(\omega) \approx 0$.
- The impurity scattering does not give the sharp decreasing of the reflectivity just above the Δ_{tun} . Instead, it decreases the gap itself.
- The coherent electron-boson scattering dominates in the superconducting state. The first derivatives from the $\gamma_{opt}^s(\omega)$ and from the $R(\omega)$ reproduce the spectral function shifted on $2\Delta_{opt}$ and *convoluted* with the Gauss distribution function $exp(-\omega^2/\Delta_{opt}^2)$ (see Fig. 9b).
- Since the frequency dependence of the coherent relaxation rate grows faster than the normal state one, and reaches its maximum value when the frequency $\omega \approx 2\Delta_{tun} + \Omega_{max}$, at this point the ratio of the $\gamma_{opt}^s(\omega)/\gamma_{opt}^n(\omega)$ will exhibit a maximum and reflectivities ratio $R_s(\omega)/R_n(\omega)$ will exhibit a minimum.

Finally, let us make the simple acceptance test for the presented above visual accessibility procedure. The test spectral function has a long history. At that old time, when people did not distinguish between the *effective* scattering rate $\gamma_{eff}(\omega)$ and the *optical* one $\gamma_{opt}(\omega)$, Collins *et al* [22] interpreted the high energy asymptotic behaviour of the $\gamma_{opt}(\omega)$ (see Fig. 2) in terms of its step-like effective counterpart $\gamma_{eff}(\omega)$ (5, 30). As the result, they arrived at the spectral function having a long tail up to the very high frequency (see Fig. 9d, inset). Nowadays, similar spectral functions occasionally arise in different models, since this shape suggests the spin fluctuations spectrum reported by neutron spectroscopy.

The calculations was performed in the same fashion as for model spectral function shown in Fig. 9a. The coupling constant was chosen to reproduce the value of the *tunnelling* gap $\Delta_{tun}=200 \text{ cm}^{-1}$. The values of the plasma frequency ω_{pl} and low-frequency value of the non-metallic part of the dielectric permeability ϵ_∞ were obtained by the least-square fit. The peak position had the value 330 cm^{-1} which

was close to the one in the original paper [22]. I choose the power law $1/\omega^{2.5}$ for the tail and the high energy cut-off 1600 cm^{-1} .

Let us compare the calculated curve and the experimental one. Since the low frequency bound in the model spectrum $\Omega_{min} \approx 200 \text{ cm}^{-1}$, the absorption edge takes place at $\Omega_{min} + \Delta_{tun}$ in accord with the results discussed in [26]. At second, in the region between 400 cm^{-1} and 800 cm^{-1} , where the reflectivity "integrates" the spectral function, there is a systematic shift on 140 cm^{-1} . For the compensation of this shift one has to decrease the value of tunnelling gap by a factor of two. The most important discrepancy is connected with the upper frequency bound of the single-particle relaxation, that is, with the Ω_{max} . The reflectivity ratio R_s/R_n has a minimum at 1400 cm^{-1} in comparison with the 900 cm^{-1} in the experimental one.

In conclusion, the separable d -wave model reproduce all important features of the traditional ISB s -wave one with the single exception: the resulting images of the spectral function are the convolution of the input electron-boson interaction function and the Gauss distribution $\exp(-\omega^2/\Delta^2)$.

IV. ACKNOWLEDGEMENTS

I express my deep gratitude to S.-L. Drechsler, O. V. Dolgov, E. G. Maksimov, A. Golubov, D. Rainer, M. Kubic, N. Yu. Boldyrev, V. M. Burlakov, and R. S. Gonnelli for numerous discussions, fruitful collaboration, and generous support of this work. I am deeply grateful to K.D. Schotte, K.F. Renk, E.A. Vinogradov, V.N. Agranovich, J. Fink, and V.L. Ginzburg for their stimulate decisive support during my work.

The author acknowledges gratefully for financial support of SFB 311 and 463.

- [1] Nam, S.B. (1967) Theory of electromagnetic properties of superconducting and normal systems, *Phys. Rev.* **156**, 470-493
- [2] Allen, P.B. (1971) Electron-phonon effects in the infrared properties of metals, *Phys. Rev.* **B3**, 305-320
- [3] Farnworth, B. and Timusk, T. (1976) Phonon density of states of superconducting lead, *Phys. Rev.* **B14**, 5119-5120
- [4] Shulga, S.V., Drechsler, S.-L., Fuchs, G., Müller, K.-H., Winzer K., Heinecke, M., and Krug K. (1998) Upper critical field peculiarities of superconducting $\text{YNi}_2\text{B}_2\text{C}$ and $\text{LuNi}_2\text{B}_2\text{C}$ *Phys. Rev. Lett.*, **80**, 1730-1733
- [5] Schutzmann, J., Gorshunov, B., Renk, K.F., Munzel, J., Zibold, A., Geserich, H.P., Erb, A. and Muller-Vogt G. (1992) Far-infrared hopping conductivity in the CuO chains of a single-domain $\text{YBa}_2\text{Cu}_3\text{O}_{7-d}$ crystal, *Phys. Rev.* **B46**, 512-515
- [6] Sulewski, P.E., Sievers, A.J., Buhrman, R.A., Tarascon, J.M., Greene, L.H. and Curtin, W.A. (1987) Far-infrared measurement of $\alpha^2(\omega)F(\omega)$ in superconducting $\text{La}_{1.84}\text{Sr}_{0.16}\text{CuO}_{4-y}$, *Phys. Rev.* **B35**, 5330-5333
- [7] Shulga, S.V., Dolgov, O.V., and Maksimov, E.G. (1991) Electronic states and optical spectra of HTSC with electron-phonon coupling, *Physica* **C178**, 266-274
- [8] Carbotte, J.P. (1990) Properties of boson-exchange superconductors, *Rev. Mod. Phys.* **62**, 1027-1158
- [9] Lee, W., Rainer, D. and Zimmerman, W. (1989) Holstein effect in the far-infrared conductivity of high T_c superconductors, *Physica* **C159**, 535-544
- [10] Dolgov, O.V., Golubov, A.A., and Shulga, S.V. (1990) Far infrared properties of high T_c superconductors, *Physics Letters* **A147**, 317-322
- [11] Allen, P.B. and Mitrovic, B. (1982) Theory of superconducting T_c , in *Solid State Physics* **37**, edited by Ehrenreich H., Zeitz F., and Turnbull, D., Academic publ., N.Y., 1-92
- [12] Abramowitz, M. and Stegun, I.A. (1970) *Handbook of Mathematical functions*, Dover publications, Inc., N.Y, 589-598
- [13] Marsiglio, F., Startseva, T. and Carbotte, J.P. (1998) Inversion of $\text{K}_3\text{C}_6\text{O}$ reflectance data, *Phys. Lett.* **A245**, 172-176
- [14] Vidberg, H.J. and Sirene, J. (1977) Solving the Eliashberg equations by means of N-point Pade approximants, *J. Low Temp. Phys.* **29**, 179-192
- [15] Dolgov, O.V. and Shulga, S.V. (1995) Analysis of intermediate boson spectra from FIR data for HTSC and heavy fermion systems, *J. of Superconductivity* **8**, 611-612

- [16] Degiorgi, L., Wachter, P., Gruner, G., Huang, S.-M., Wiley, J. and Kaner, R.B. (1992) Optical response of the superconducting state of K_3C_{60} and Rb_3C_{60} , *Phys. Rev. Lett* **69**, 2987-2990
- [17] Degiorgi, L., Nicol, E.J., Klein, O., Gruner, G., Wachter, P., Huang, S.-M., Wiley, J. and Kaner, R.B. (1994) Optical properties of the alkali-metal-doped superconducting fullerenes: K_3C_{60} and Rb_3C_{60} , *Phys. Rev.* **B49**, 2787-2990
- [18] Mazin, I.I., Dolgov, O.V., Golubov, A. and Shulga, S.V. (1993) Strong-coupling effects in alkali-metal-doped C_{60} , *Phys. Rev.* **B47**, 538-541
- [19] Press, V.H., Teukolsky, S.A., Vetterling, W.T., and Flannery, B.P. (1992) *Numerical recipes*, sec. 18.4-18.7, Cambridge uni. press, N.Y, 795-817
- [20] Joyce, R.R. and Richards, P.L. (1970) Phonon contribution to the far-infrared absorptivity of superconducting and normal lead, *Phys. Rev. Lett.* **24**, 1007-1011
- [21] Farnworth, B. and Timusk, T. (1974) Far-infrared measurement of the phonon density of states of superconducting lead, *Phys. Rev.* **B10**, 2799-2802
- [22] Collins, R.T., Schlesinger, Z., Holtzberg, F., Chaudhary, P. and Field, C. (1989) Reflectivity and conductivity of $YBa_2Cu_3O_7$, *Phys. Rev.* **B39**, 6571-6574
- [23] Sulewski, P.E., Sievers, A.J., Maple, M.B., Torikachvili, M.S., Smith, J.L. and Fisk, Z. (1988) Far-infrared absorptivity of UPt_3 , *Phys. Rev.* **B38**, 5338-5352
- [24] Burlakov, V.M., Shulga, S.V., Keller, J. and Renk, K.F. (1992) Evidence for a Fano-type interaction of infrared active phonons with electronic excitations in $Tl_2Ba_2Ca_2Cu_3O_{10}$, *Physica* **C190**, 304-308
- [25] Basov, D.N., Liang, R., Dabrowski, B., Bonn, D.A., Hardy, W.N. and Timusk, T. (1996) Pseudogap and charge dynamics in CuO_2 planes in $YBaCO$, *Phys. Rev. Lett.* **77**, 4090-4093
- [26] Kamaras, K., Herr, S.L., Porter, C.D., Tache, N., Tanner, D.B., Etemad, S., Venkatesan, T., Chase, E., Inam, A., Wu, X.D., Hegde, M.S. and Dutta, B. (1991) In a clean high- T_c superconductor you do not see the gap, *Phys. Rev. Lett.* **64**, 84-87
- [27] Maksimov, E. G., Rashkeev, S. N., Savrasov, S. Yu., Uspenskii, Yu. A. (1989) Microscopic studies of the optical spectra of $YBa_2Cu_3O_7$ *Phys. Rev. L* **63**, 1880-1883
- [28] Dervenagas, P., Bullock, M., Zarestky, J., Canfield, P., Cho, B.K., Harmon, B., Goldman, A.I. and Stassis, C. (1995) Soft phonons in superconducting $LuNi_2B_2C$, *Phys. Rev.* **B52**, R9839-R9842
- [29] Kawano, H., Yoshizawa, H., Takeya, H., Kadowaki K. (1997) New phonon peak in superconducting state of YNi_2B_2C *Physica* **C282-287** 1055-1056
- [30] Kawano, H., Yoshizawa, H., Takeya, H., Kadowaki K.(1996) Anomalous photon scattering below T_c in YNi_2B_2C *Phys. Rev. Lett.* **77** 4628-4631
- [31] Schachinger, E., Carbotte, J.P. and Marsiglio, F. Effect of suppression of the inelastic scattering rate on the penetration depth and conductivity in a $d_{x^2-y^2}$ superconductor, *Phys. Rev.* **B56**, 2738-2750
- [32] Zhao, G.L., Browne, D. A. and Callaway, J. (1995) Quasiparticle spectrum in superconducting $YBa_2Cu_3O_7$, *Phys. Rev.* **B52**, 16217-16222